

## List of changes

|    |   |   |
|----|---|---|
|    | Deleted: and spaceborne                           | 1 |
|    | Deleted: of                                       | 1 |
|    | Deleted: (TC4)                                    | 1 |
| 5  | Added:  | 2 |
|    | Replaced: enhanced by                             | 2 |
|    | Added: capability                                 | 2 |
|    | Replaced: The retrieval of rain rate from a pr... | 2 |
|    | Deleted: reduction of                             | 2 |
| 10 | Added: , or calculated from sea surface wi...     | 2 |
|    | Replaced: Estimates of PIA are                    | 2 |
|    | Replaced: a significant improvement               | 2 |
|    | Replaced: , with                                  | 3 |
|    | Added: , aims                                     | 3 |
| 15 | Deleted: ,  | 3 |
|    | Replaced: 9.6 GHz                                 | 3 |
|    | Replaced: a less attenuated                       | 3 |
|    | Added: ,  | 3 |
|    | Replaced: -frequency radar                        | 3 |
| 20 | Added: and the retrieval of more complex ...      | 3 |
|    | Added: at temperatures greater than 0°C           | 5 |
|    | Added: In stratiform precipitation we assu ...    | 5 |
|    | Added: cloud                                      | 5 |
|    | Added: As a result of the uncertain presen ...    | 5 |
| 25 | Replaced: measurements                            | 6 |
|    | Added: Here we present a general descript ...     | 6 |
|    | Replaced: $\mathbf{x}^\alpha$                     | 6 |
|    | Added: in which the diagonal elements are ...     | 6 |
|    | Replaced: provides the capability to apply        | 6 |
| 30 | Replaced: flatness                                | 6 |
|    | Replaced: ness                                    | 6 |
|    | Replaced: to reduce the effect of observation ... | 6 |
|    | Added: Additionally, profiles of retrieved ...    | 6 |
|    | Added: corrected for air density through t ...    | 7 |
| 35 | Added: While a prior $R$ is not strictly nec ...  | 7 |
|    | Added: Additional state variables increase ...    | 7 |
|    | Replaced: .                                       | 7 |
|    | Replaced: assuming that $N_w$ is constant and ... | 7 |
|    | Added: constant everywhere                        | 7 |
| 40 | Replaced: with the effect                         | 7 |
|    | Replaced: in fewer iterations                     | 7 |
|    | Added: While in moderate stratiform rain ...      | 7 |
|    | Added: $R$ is therefore represented as the c ...  | 7 |
|    | Added: and uncertainties,                         | 7 |
| 45 | Replaced: representation                          | 7 |
|    | Deleted: with $n$ elements, or pixels,            | 7 |
|    | Deleted: full                                     | 8 |
|    | Replaced: $N_w$ is assumed constant with heig ... | 8 |

|    |   |    |
|----|---|----|
|    | Deleted: At moderate rain rates, we expect...                       | 8  |
|    | Deleted: however, at low rain rates $R$ may ...                     | 8  |
|    | Deleted: Therefore to reduce noise and ens ...                      | 8  |
|    | Added: , with a spacing of 300m                                     | 8  |
| 5  | Added: in this study  | 8  |
|    | Added: Stratiform precipitation                                     | 8  |
|    | Replaced: employ a simplified representation of                     | 8  |
|    | Added: in stratiform precipitation                                  | 8  |
|    | Added: Melting of graupel and hail, usual ...                       | 8  |
| 10 | Added: Matrosov (2008)  | 8  |
|    | Deleted: Matrosov (2008)  | 8  |
|    | Added: and the two-way path length $X_m$ ...                        | 8  |
|    | Added: the melting layer extinction coeffi ...                      | 8  |
|    | Added: is   | 8  |
| 15 | Added: and $0.04 \text{ dB km}^{-1} (\text{mm h}^{-1})^{-1}$ at ... | 8  |
|    | Added: . The estimated attenuation throug ...                       | 8  |
|    | Added: (Matrosov, 2008), and is not modi ...                        | 8  |
|    | Deleted: (Matrosov 2008)  | 8  |
|    | Deleted: the  | 9  |
| 20 | Replaced: 1.0 km  | 9  |
|    | Added: for 94 GHz and 9.6 GHz radars                                | 9  |
|    | Deleted: as drop sizes approach the radar w ...                     | 9  |
|    | Added: At 94 GHz the uncertainty of assu ...                        | 9  |
|    | Replaced: Scattering and attenuation effects ...                    | 9  |
| 25 | Added: ( $Z_a$ )  | 9  |
|    | Replaced: on radar and lidar backscatter can ...                    | 9  |
|    | Replaced: . Radar reflectivity enhancement d ...                    | 9  |
|    | Added: As for radar reflectivity, the uncert ...                    | 9  |
|    | Replaced: , so that   | 10 |
| 30 | Replaced: is applied only at moderate to hea ...                    | 10 |
|    | Replaced: scaled to account for air density c ...                   | 10 |
|    | Replaced: uncertainties in the observational ...                    | 10 |
|    | Replaced: measurement errors  | 10 |
|    | Added: and the estimated uncertainties in ...                       | 10 |
| 35 | Replaced: $1.0 \text{ ms}^{-1}$                                     | 10 |
|    | Deleted: , so that the uncertainty in radar re ...                  | 10 |
|    | Added: We have found that the weighting ...                         | 10 |
|    | Deleted: liquid water, and especially by                            | 11 |
|    | Deleted: ,  | 11 |
| 40 | Added: rate   | 11 |
|    | Added: apparent   | 11 |
|    | Replaced: combine   | 12 |
|    | Replaced: In each case the retrieval is evalua ...                  | 13 |
|    | Deleted: in this case   | 13 |
| 45 | Replaced: precipitating stratiform cloud                            | 13 |
|    | Added: , which is primarily detected by th ...                      | 13 |
|    | Added: evident  | 13 |
|    | Added: 94 GHz   | 13 |
|    | Replaced: 60 dB   | 13 |

|    |  |    |
|----|--|----|
|    | Replaced: these                                  | 13 |
|    | Added: close to                                  | 13 |
|    | Added: some                                      | 13 |
|    | Replaced: , while                                | 13 |
| 5  | Replaced: and decreases                          | 13 |
|    | Deleted: Comparisons of the independent          | 13 |
|    | Deleted: with those                              | 13 |
|    | Added: generally                                 | 13 |
|    | Added: with independent observations             | 13 |
| 10 | Added: and mean Doppler velocity is ...          | 14 |
|    | Deleted: Moderate rain profiles with signifi ... | 14 |
|    | Added: The averaged vertical profiles of t ...   | 14 |
|    | Deleted: We use the                              | 14 |
|    | Deleted: of $R-N_w$                              | 14 |
| 15 | Replaced: illustrate                             | 14 |
|    | Replaced: ZvPIA                                  | 14 |
|    | Added: and uncertainties                         | 14 |
|    | Added: (Fig. 4)                                  | 14 |
|    | Added: in the moderate rain regime               | 14 |
| 20 | Added: significantly                             | 14 |
|    | Replaced: large                                  | 14 |
|    | Replaced: in                                     | 14 |
|    | Replaced: tends to underestimate                 | 14 |
|    | Added: , with the exception of the strongly ...  | 14 |
| 25 | Replaced: PIA                                    | 14 |
|    | Replaced: and rain rate are                      | 14 |
|    | Added: er than that estimated from ZvPIA         | 14 |
|    | Deleted: s                                       | 14 |
|    | Deleted: ward                                    | 14 |
| 30 | Deleted: ing                                     | 14 |
|    | Replaced: variables                              | 14 |
|    | Added: leads to a                                | 14 |
|    | Added: ly  | 14 |
|    | Replaced: d                                      | 14 |
| 35 | Replaced: this frequency                         | 14 |
|    | Replaced: $N_w$ is underestimated                | 14 |
|    | Deleted: Selected profiles of retrieved and ...  | 14 |
|    | Added: $R$ and                                   | 15 |
|    | Deleted: s                                       | 15 |
| 40 | Added: s   | 15 |
|    | Deleted: strong                                  | 15 |
|    | Replaced: a PIA constraint                       | 16 |
|    | Replaced: is close to                            | 16 |
|    | Added: s   | 16 |
| 45 | Added: A secondary mode with $N_w$ close ...     | 16 |
|    | Replaced: We                                     | 16 |
|    | Added: as a function of both $D_0$               | 16 |
|    | Added: for a case                                | 16 |
|    | Replaced: ,including                             | 16 |

|    |  |    |
|----|--|----|
|    | Deleted: varying                                 | 16 |
|    | Added: where total attenuation is close to zero  | 16 |
|    | Replaced: profiles of moderate                   | 16 |
|    | Added: DSDs with                                 | 16 |
| 5  | Deleted: number                                  | 16 |
|    | Added: is equal to the prior                     | 16 |
|    | Replaced: very light rain from melting ice       | 16 |
|    | Replaced: stratiform                             | 16 |
|    | Deleted: :00                                     | 16 |
| 10 | Deleted: :30                                     | 16 |
|    | Deleted: ice                                     | 16 |
|    | Replaced: decrease                               | 16 |
|    | Deleted: and                                     | 16 |
|    | Replaced: zero                                   | 17 |
| 15 | Replaced: significant evaporation                | 17 |
|    | Deleted: significant                             | 17 |
|    | Replaced: representation                         | 17 |
|    | Deleted: near the surface                        | 17 |
|    | Deleted: very                                    | 17 |
| 20 | Added: 4 km                                      | 17 |
|    | Replaced: ;                                      | 17 |
|    | Added: however, the averaged vertical pro ...    | 17 |
|    | Replaced: may                                    | 17 |
|    | Deleted: n accurate                              | 17 |
| 25 | Added: from liquid clouds                        | 17 |
|    | Added: a   | 17 |
|    | Replaced: 6                                      | 17 |
|    | Replaced: 6                                      | 17 |
|    | Replaced: and                                    | 17 |
| 30 | Added: , as discussed in Section 2.2, lidar ...  | 18 |
|    | Replaced: Hence we                               | 18 |
|    | Deleted: from collision and coalescence          | 18 |
|    | Replaced: 6                                      | 18 |
|    | Replaced: in                                     | 18 |
| 35 | Replaced: were estimated for                     | 18 |
|    | Replaced: accordingly, the drops                 | 18 |
|    | Deleted: ,                                       | 18 |
|    | Replaced: At 1 km above sea level t              | 18 |
|    | Replaced: .                                      | 18 |
| 40 | Replaced: The                                    | 18 |
|    | Deleted: exceptionally                           | 18 |
|    | Deleted: ; this is because at the small drop ... | 18 |
|    | Replaced: ; however, while the                   | 18 |
|    | Added: , peaks associated with the heavie ...    | 18 |
| 45 | Added: The vertical structure of 94 GHz a ...    | 18 |
|    | Replaced: The                                    | 18 |
|    | Replaced: closely                                | 18 |
|    | Deleted: The forward-modelled 94 GHz an ...      | 18 |
|    | Replaced: $Z_V$ retrieves similar $D_0$          | 18 |

|    |   |    |
|----|---|----|
|    | Replaced: may be  | 18 |
|    | Deleted: noisy  | 19 |
|    | Deleted: The forward-modelled PIA is 0 dB ...               | 19 |
|    | Replaced: est profiles                                      | 19 |
| 5  | Replaced: In warm rain, we have retrieved                   | 19 |
|    | Added: several orders of magnitude greater ...              | 19 |
|    | Replaced: in rain rates                                     | 19 |
|    | Deleted: ,  | 19 |
|    | Deleted: of warm rain from liquid clouds                    | 19 |
| 10 | Replaced: We compare the                                    | 19 |
|    | Replaced: measurements                                      | 19 |
|    | Deleted: on 22 July 2007                                    | 19 |
|    | Added: rain   | 19 |
|    | Deleted: retrievals   | 19 |
| 15 | Deleted: the  | 19 |
|    | Deleted: profiles   | 20 |
|    | Deleted: of the ZPIA retrieval                              | 20 |
|    | Added: due to complete extinction of the ...                | 20 |
|    | Deleted: the unattenuated                                   | 20 |
| 20 | Added: measurements alone                                   | 20 |
|    | Added: is estimated   | 20 |
|    | Replaced: illustrates                                       | 20 |
|    | Added: with large retrieval uncertainty,                    | 20 |
|    | Deleted: ZvPIA  | 20 |
| 25 | Replaced: be  | 20 |
|    | Added: Retrieving vertical profiles of $N_w$                | 20 |
|    | Added: We have demonstrated the retrieval ...               | 20 |
|    | Added: It is of interest to represent change ...            | 20 |
|    | Added: where $\overline{N_w}$ is the average $N_w$ thro ... | 20 |
| 30 | Added: A retrieval in which $N_w$ is represe ...            | 21 |
|    | Added: With an additional degree of freed ...               | 21 |
|    | Replaced: a   | 21 |
|    | Replaced: airborne Doppler radar                            | 21 |
|    | Deleted: global   | 21 |
| 35 | Replaced: improving   | 21 |
|    | Replaced: a less  | 21 |
|    | Replaced: 9.6 GHz Doppler radar.                            | 21 |
|    | Replaced: at strongly                                       | 21 |
|    | Added: frequencies  | 21 |
| 40 | Replaced: an estimate of path-integrated atte ...           | 21 |
|    | Replaced: by the profile of mean Doppler vel ...            | 21 |
|    | Replaced: The latter has                                    | 21 |
|    | Added: , where PIA is more difficult to est ...             | 21 |
|    | Replaced: measurements from                                 | 22 |
| 45 | Replaced: from  | 22 |
|    | Replaced: in profiles with                                  | 22 |
|    | Deleted: falling  | 22 |
|    | Replaced: in rain from                                      | 22 |
|    | Replaced: used  | 22 |

|    |   |    |
|----|---|----|
|    | Added: In many contexts collision–...         | 22 |
|    | Deleted: Mean Doppler velocity provides a...  | 22 |
|    | Replaced: In                                  | 22 |
|    | Replaced: of using                            | 22 |
| 5  | Added: for                                    | 22 |
|    | Added: without PIA                            | 22 |
|    | Added: constant, especially for stratiform... | 22 |
|    | Added: backscatter                            | 22 |
|    | Added: A robust method of using Doppler...    | 22 |
| 10 | Added: apparent                               | 22 |
|    | Added: We have demonstrated the contrib...    | 23 |
|    | Replaced: EarthCARE synergy retrievals wil... | 23 |
|    | Replaced: clouds and precipitation            | 23 |
|    | Deleted: Mean Doppler velocity provides a...  | 23 |
| 15 | Added: Future work will focus on underst...   | 23 |
|    | Deleted: from Doppler radar                   | 23 |
|    | Deleted: , aerosols                           | 23 |
|    | Added: We are grateful to Alain Protat and... | 23 |

## Improved rain-rate and drop-size retrievals from airborne and spaceborne Doppler radar

Shannon L. Mason<sup>1,2</sup>, J. Christine Chiu<sup>1,2</sup>, Robin J. Hogan<sup>1,3</sup>, and Lin Tian<sup>4,5</sup>

<sup>1</sup>Department of Meteorology, University of Reading, Reading, UK

<sup>2</sup>National Centre for Earth Observation, University of Reading, Reading, UK

<sup>3</sup>European Centre for Medium-range Weather Forecasts, Reading, UK

<sup>4</sup>NASA Goddard Space Flight Centre, Greenbelt MD, USA

<sup>5</sup>Morgan State University, Baltimore MD, USA

*Correspondence to:* Shannon Mason (s.l.mason@reading.ac.uk)

**Abstract.** Satellite radar remote-sensing of rain is important for quantifying ~~of~~ the global hydrological cycle, atmospheric energy budget, and many microphysical cloud and precipitation processes; however, radar estimates of rain rate are sensitive to assumptions about the raindrop size distribution. The upcoming EarthCARE satellite will feature a 94GHz Doppler radar alongside lidar and radiometer instruments, presenting opportunities for enhanced global retrievals of the rain drop size distribution.

In this paper we demonstrate the capability to retrieve both rain rate and a parameter of the rain drop size distribution from an airborne 94GHz Doppler radar using CAPTIVATE, the variational retrieval algorithm developed for EarthCARE radar–lidar synergy. For a range of rain regimes observed during the Tropical Composition, Cloud and Climate Coupling (TC4) field campaign in the eastern Pacific in 2007, we explore the contributions of Doppler velocity and path-integrated attenuation (PIA) to the retrievals, and evaluate the retrievals against independent measurements from a second, less attenuated, Doppler radar aboard the same aircraft. Retrieved drop number concentration varied over five orders of magnitude between

light rain from melting ice, and warm rain from liquid clouds. Doppler velocity can be used to estimate rain rate over land, and retrievals of rain rate and drop number concentration are possible in profiles of light rain over land; in moderate warm rain, drop number concentration can be retrieved without Doppler velocity. These results suggest that EarthCARE rain retrievals ~~enhanced by~~ ~~facilitated by~~ Doppler radar ~~capability~~ will make substantial improvements to the global understanding of the interaction of clouds and precipitation.

## 1 Introduction

Satellite remote sensing of rain is important for quantifying the global water and energy cycles. Even light rain and drizzle make significant contributions to global precipitation (Haynes et al., 2009; Berg et al., 2010; Behrangi et al., 2012), while profiling measurements can be used to estimate the vertical transfer of latent heat (Nelson et al., 2016) and microphysical processes (Lebsock et al., 2013; Wood et al., 2009). The intensity and drop size distribution (DSD) of rain are related to persistent errors in weather and climate models, which frequently produce excess drizzle from shallow maritime clouds (Stephens et al., 2010; Abel and Boutle, 2012). Improved instrumentation and retrieval algorithms for the satellite remote sensing of rain are therefore priorities for earth observation and model evaluation.

The first spaceborne cloud and precipitation radars facilitated significant advances in the detection and measurement of rain, especially over the oceans. The 14 GHz precipitation radar aboard the tropical rainfall measurement mission (TRMM; Kummerow et al., 1998) measured moderate and heavy precipitation in the tropics. The more sensitive 94 GHz cloud profiling radar aboard CloudSat (Stephens et al., 2002) is capable of measuring very frequent light rainfall not detected by TRMM, which amounts to 10% of the total tropical maritime precipitation (Berg et al., 2010). CloudSat measurements of the profile of light rain have shown that around 70% of marine precipitation falls as drizzle, 50–80% of which evaporates before reaching the surface (Rapp et al., 2013). The high sensitivity of 94 GHz radar allows profiling measurements of light rain and drizzle, at the cost of significant radar attenuation in moderate to heavy rain.

The retrieval of rain rate from a profile of apparent radar reflectivity requires knowledge of the attenuation of the radar beam. ~~To reliably estimate rain rates from profiles of radar reflectivity, the attenuation of the radar beam due to liquid hydrometeors must be quantified.~~ The path-integrated attenuation (PIA) can be estimated from the ~~reduction of~~ the ocean surface backscatter relative to nearby clear-sky profiles (Meneghini et al., 1983), ~~or calculated from sea surface wind speed and temperature~~ (Haynes et al., 2009). ~~Estimates of PIA are~~ ~~PIA estimated from this surface reference method is~~ used in the rain retrieval algorithms of both TRMM (Iguchi et al., 2000; Meneghini and Liao, 2000) and CloudSat (L'Ecuyer and Stephens, 2002; Haynes et al., 2009; Lebsock and L'Ecuyer, 2011) over the ocean; however, the surface backscatter over the land is much more variable and difficult to characterise. Consequently operational CloudSat data products currently provide only rain detection over land, and not rain rate estimates (e.g. Haynes et al., 2009; Lebsock and L'Ecuyer, 2011). Additional radar measurements that facilitate rain rate estimates over land would offer ~~a significant improvements~~ ~~significant improvements~~ over existing satellite capabilities.

Estimates of rain rate from limited radar measurements rely upon assumptions about the rain DSD. While the statistical properties of rain DSDs have been found to be broadly consistent and robust over time, whether measured in situ (Marshall and Palmer, 1948; Tokay and Short, 1996) or estimated by radar remote-sensing (Wilson et al., 1997; Illingworth and Blackman, 2002), the instantaneous microphysical properties of rain are observed to vary over many orders of magnitude (Testud et al., 2001). Assumptions about the drop number concentration in particular have been identified as a major source of uncertainty in TRMM and CloudSat estimates of rain rate (Iguchi et al., 2009; Lebsock and L'Ecuyer, 2011). To improve upon the uncertainties of satellite remote-sensed rain rate, there is a need for additional radar measurements with which to better characterise the rain DSD.

There are two approaches to improving rain retrievals with additional observations from satellite radars, both to assist in estimating rain rate over land, and to better constrain the rain DSD. The recent global precipitation measurement mission (GPM; Hou et al., 2014), ~~with uses~~ the first dual-frequency radar in space, ~~aims~~ to exploit differences in non-Rayleigh scattering at 35 GHz and 14 GHz, to better constrain the rain DSD over land and ocean (e.g. Rose and Chandrasekar, 2006). Another approach is to use Doppler radar to measure the terminal fallspeed of raindrops, which is related to drop size. The Doppler spectrum has been used in ground-based radar retrievals to resolve vertical air motion (Atlas et al., 1973; Firda et al., 1999; O'Connor et al., 2005), distinguish cloud from precipitation (Frisch et al., 1995; Luke and Kollias, 2013), and to understand warm rain processes (Kollias et al., 2011b, a). Unfortunately in spaceborne radar applications the Doppler spectrum is broadened by the lateral motion of the radar platform with respect to the scattering hydrometeors (Illingworth et al., 2015), which distorts the higher moments of the Doppler spectrum; consequently, only radar reflectivity, PIA, and mean Doppler velocity measurements are useful for spaceborne Doppler radar retrievals.

The EarthCARE satellite will feature a 94 GHz Doppler radar along with lidar and radiometers, for synergistic retrievals of clouds, aerosols and precipitation (Illingworth et al., 2015). In this study we develop a method for making an improved estimate of rain rate by simultaneously retrieving information about the DSD from an airborne 94 GHz Doppler cloud radar. We use a variational retrieval methodology developed for radar–lidar synergy from EarthCARE (Illingworth et al., 2015), and exploit mean Doppler velocity to retrieve the raindrop number concentration. NASA's high-altitude ER-2 aircraft provides an ideal platform for satellite instruments and retrievals; we use ER-2 measurements from the Tropical Composition, Clouds and Climate Coupling field campaign (TC4) off Costa Rica and Panama in 2007 (Toon et al., 2010). A second ~~9.6 GHz~~~~40 GHz~~ Doppler radar aboard ER-2 provides independent measurements at ~~a less attenuated~~~~an unattenuated~~ wavelength, with which to evaluate the retrievals.

The structure of this paper is as follows. We first describe the aircraft measurements, the synergistic classification of hydrometeors, and the retrieval method (Section 2). The ambiguities of retrieving rain rate from attenuated radar profiles are discussed using synthetic measurements (Section 3), before 94 GHz radar retrievals of rain rate and drop number concentration are presented for three case studies, and the retrievals are evaluated against independent radar measurements at an unattenuated wavelength (Section 4). We briefly consider applications of the dual-frequency ~~radar-radar~~ retrievals (Section 5), ~~and the retrieval of more complex variations in the DSD through the vertical profile~~ (Section 6), before summarising our key findings with a view to applications to EarthCARE retrievals (Section 7).

## 2 Data and retrieval methodology

### 2.1 Measurements used in the retrieval

The observations are from NASA's high altitude ER-2 aircraft during the TC4 experiment conducted over the tropical eastern Pacific in July and August 2007 (Toon et al., 2010). ER-2 flies above the tropopause at an altitude of 20 km with a cruise speed  
5 around  $200\text{ms}^{-1}$ . We analyse measurements from straight flight legs over the ocean, and average all measurements over 5 s intervals, so that each pixel of radar–lidar data has a 1 km along-track footprint.

The 94 GHz (3.2 mm wavelength) cloud radar system (CRS; Li et al., 2004) and 9.6 GHz (3.1 cm wavelength) ER-2 Doppler radar (EDOP; Heymsfield et al., 1996) measure radar reflectivity factor and mean Doppler velocity with a vertical gate spacing of 37.5 m. The 94 GHz radar reflectivity factor is calibrated against the 9.6 GHz radar near cloud-top (McGill, 2004), and the  
10 mean Doppler velocity measurements are calibrated using the surface signal (Li et al., 2004). The path-integrated attenuation (PIA) of the 94 GHz radar is estimated over the ocean using the surface reference technique (L'Ecuyer and Stephens, 2002; Lebsock and L'Ecuyer, 2011). In this study we focus on the retrieval of rain from the 94 GHz cloud radar, and use the 9.6 GHz radar for evaluation.

The cloud physics lidar (CPL; McGill et al., 2002) measures attenuated backscatter at 355 nm, 532 nm and 1064 nm, with  
15 linear polarisation ratio measured at the 1064 nm wavelength. In this study the 532 nm attenuated backscatter is used in the classification scheme to detect cloud top and to retrieve overlying ice cloud and liquid layers when the lidar signal is not fully attenuated.

The MODIS airborne simulator (MAS; King et al., 1996) and MODIS/ASTER airborne simulator (MASTER; Hook et al., 2001) imaging radiometers measure infrared (IR) and visible channels. Three visible channels are combined to create composite  
20 images of the case studies. Due to a failure in the MAS instrument, the MASTER instrument flew aboard ER-2 as a replacement after 29 July 2007 (Toon et al., 2010); the channels used in this study are common to both instruments.

Supplementary environmental data are required to complete the retrieval. Atmospheric temperature, humidity and ozone concentration are used to classify hydrometeor thermodynamic phase and estimate radar and lidar attenuation due to atmospheric gases. These variables are interpolated onto the flight track from the European Centre for Medium-Range Weather  
25 Forecasts (ECMWF) Interim Re-Analysis (ERA-Interim; Dee et al., 2011).

### 2.2 Target classification

Prior to the retrieval the contents of each pixel are classified based on a synthesis of radar and lidar measurements. We exploit the instruments' complementary sensitivities to different classes of hydrometeors to infer the presence of liquid cloud, rain and drizzle, and ice. This approach to radar–lidar target classification is similar to that described for CloudSat–CALIPSO in  
30 Ceccaldi et al. (2013), however the categories are simplified in this analysis.

A trade-off in radar and lidar remote sensing is that the hydrometeors with the strongest backscatter also strongly attenuate the beam, weakening its penetration. The sensitivity of lidar to small ice crystals and cloud droplets makes it suited to detecting optically thin ice and liquid cloud, but lidar is therefore quickly attenuated in all but the optically thinnest clouds. In contrast,

cloud radar is most sensitive to large hydrometeors such as ice aggregates and raindrops, and becomes fully attenuated in heavy rain. With the synergy of the two instruments we can use radar to detect optically thick clouds and light to moderate rain, while lidar detects optically thin ice and liquid cloud-tops missed by the radar.

The thermodynamic phase of targets is primarily determined by the atmospheric temperature from reanalysis, with further distinctions made using thresholds of radar and lidar measurements. At temperatures colder than  $-40^{\circ}\text{C}$  all targets are classified as ice, and at all temperatures warmer than  $0^{\circ}\text{C}$  as “warm” liquid cloud or precipitation. Rain and drizzle is inferred at temperatures greater than  $0^{\circ}\text{C}$  from radar reflectivities greater than  $-15\text{ dBZ}$  (as in Haynes et al., 2011, and others), and may be colocated with warm liquid clouds detected by lidar. In stratiform precipitation we assume that the transition from ice to liquid precipitation occurs in a shallow melting layer (see Section 2.3.4); however, in convective precipitation strong attenuation due to melting hail and tends to extinguish the 94 GHz radar. Between  $-40^{\circ}\text{C}$  and  $0^{\circ}\text{C}$  the thermodynamic phase of cloud water can be ice, supercooled liquid or, where the two coexist, mixed-phase. First all targets detected by radar are classified as containing ice, due to the sensitivity of that instrument to the largest particles. Then liquid and ice as detected by lidar are distinguished based on the vertical gradient of lidar backscatter, which is higher in liquid cloud (Ceccaldi et al., 2013); this method of distinguishing liquid cloud is consistent with the method of Yoshida et al. (2010) using the lidar depolarization ratio. Where radar detects ice and lidar detects liquid, mixed-phase cloud is diagnosed.

The vertical structure and thermodynamic phase of clouds provide constraints on the retrieval of cloud and precipitation properties, but the entire profile is frequently not detectable by both instruments. Therefore the lidar is used to retrieve liquid clouds, but the presence of liquid cloud droplets is an uncertainty in the classification scheme where only radar measurements are available. The lidar is included in the present work for its contribution to the classification of cloud through the vertical profile, and for measuring the water content at cloud-top; however, the radar is the dominant instrument for the retrieval of rain. As a result of the uncertain presence of liquid clouds within rainy profiles, the path-integrated attenuation of the radar that is attributed to rain may be partially due to undiagnosed liquid cloud. Finally, in profiles where the radar is fully attenuated by heavy rain, we assume that rain is continuous to the surface.

### 2.3 Retrieval methodology

Radar–lidar retrievals of profiles of rain and ice cloud are made using the Clouds Aerosols and Precipitation from multiple Instruments using a Variational TEchnique (CAPTIVATE) algorithm, an earlier version of which was outlined in Illingworth et al. (2015). In this section we first describe the CAPTIVATE framework, then the main components pertinent to this study: the cost function, the state vector for rain, and the radar forward model. The retrieval is made by iteratively minimizing the cost function to find the state vector that corresponds to the smallest difference between observed and forward-modelled measurements. The state vector consists of the quantities or parameters of the rain DSD selected as retrieved variables. The forward models are used to estimate the measured variables given the state; the relevant measurements are radar reflectivity factor, PIA, and mean Doppler velocity. In this study we focus on the rain retrieval; details for other hydrometeors will be provided in subsequent papers.

### 2.3.1 Retrieval framework

The CAPTIVATE algorithm provides a framework for a variational, or optimal estimation, approach (Rodgers, 2000) to the inverse retrieval of the profiles of rain, ice and snow, liquid cloud and aerosols from one or more vertically-pointing active and passive instruments. CAPTIVATE is novel in that the measurements used and state variables retrieved are easily configurable, so that the same retrieval algorithm can be applied to spaceborne, airborne and ground-based [measurements applications](#). The treatment of retrieved state variables and the vertical representation of each class of hydrometeor can also be modified as appropriate. The variational approach allows for a robust treatment of uncertainties in the retrieval, subject to the appropriate selection of observational uncertainties, forward-model errors and physical constraints.

### 2.3.2 Cost function and minimization

Here we present a general description of the CAPTIVATE retrieval; justifications for the settings used in study are made in later subsections. The retrieval is made for each profile by iterating to find a state vector that minimizes a cost function, given by

$$J = \frac{1}{2} \delta \mathbf{y}^T \mathbf{R}^{-1} \delta \mathbf{y} + \frac{1}{2} \delta \mathbf{x}^T \mathbf{B}^{-1} \delta \mathbf{x} + J_c(\mathbf{x}) \quad (1)$$

where  $\delta \mathbf{y} = \mathbf{y} - \mathbf{y}^f$  is the difference between the observed ( $\mathbf{y}$ ) and forward-modelled ( $\mathbf{y}^f$ ) measurements;  $\mathbf{R}$  is the error covariance matrix of  $\delta \mathbf{y}$ , the sum of the error covariance matrices of the observations and the forward model;  $\delta \mathbf{x} = \mathbf{x} - \mathbf{x}^a$  is the difference between the state ( $\mathbf{x}$ ) and its a priori estimate ( $\mathbf{x}^a$ ), and  $\mathbf{B}$  is the error covariance matrix of  $\mathbf{x}^a$  ~~the a priori in which the diagonal elements are the error variances of  $\mathbf{x}$ ; and  $J_c(\mathbf{x})$  provides the capability to apply~~ ~~represents the flatness~~ ~~physical and smoothness~~ ~~constraints to reduce the effect of observational noise on the state vector (Twomey, 1977).~~ ~~on the state vector.~~ Additionally, profiles of retrieved variables can be represented smoothly as a set of cubic spline basis functions (Hogan, 2007, and in Section 2.3.3). The minimization of the cost function is carried out by iterating on the state vector beginning from the priors, in the direction of the first and second derivatives of the cost function (the Levenberg-Marquadt method; Rodgers, 2000).

### 2.3.3 Rain state variables

The rain DSD is given by a normalized Gamma function, of the form

$$N(D) = N_w \frac{\Gamma(4)}{3.67^4} \frac{(3.67 + \mu)^{4+\mu}}{\Gamma(4 + \mu)} \left( \frac{D}{D_0} \right)^\mu \exp\left( \frac{-(3.67 + \mu)D}{D_0} \right). \quad (2)$$

This formulation is a function of three independent, physically meaningful parameters for the shape  $\mu$ , median drop size  $D_0$ , and drop number concentration  $N_w$  of the DSD (Testud et al., 2001; Illingworth and Blackman, 2002). The shape factor  $\mu$  is of secondary importance to  $D_0$  and  $N_w$  in terms of the radar reflectivity (Testud et al., 2001), and is poorly constrained by observations (e.g. Moisseev and Chandrasekar, 2007). In this retrieval we use  $\mu = 5$ , a value derived from both radar and distrometer studies (Wilson et al., 1997; Illingworth and Blackman, 2002). This simplifies the DSD to a 2-parameter function

of  $D_0$  and  $N_w$ . The uncertainty due to the assumption of fixed- $\mu$  DSD is estimated to be  $\pm 15\%$  of the rain rate (Wilson et al., 1997), and is included in the uncertainty estimates of the retrieved quantities.

Our primary state variable is the rain rate,

$$R = \frac{\rho_w \pi}{6} \int_0^{\infty} N(D) D^3 v(D) dD \quad [\text{kg m}^{-2} \text{s}^{-1}], \quad (3)$$

5 from the third moment of the DSD where  $\rho_w$  is the density of liquid water,  $v(D)$  is the raindrop terminal velocity as a function of drop size from Beard (1976) corrected for air density through the vertical profile. Hereafter we scale  $R$  by a factor of 3600 to express rain rate in units of  $\text{mm h}^{-1}$ . For all retrievals a prior  $R$  of  $0.1 \text{ mm h}^{-1}$  is used. While a prior  $R$  is not strictly necessary, it is applied in combination with a large prior variance ( $\sigma(\ln R) = 4.0$ ), such that the retrieved  $R$  is relatively insensitive to the prior unless the retrieval is poorly constrained by observations. We note that this value for the prior variance implies that before  
10 the measurements are taken we assume there is a 44% chance of  $R$  lying between  $0.01$  and  $1.0 \text{ mm h}^{-1}$ , and a 56% chance  $R$  is outside these limits.

The second state variable is  $N_w$ , so that one state variable is an integral over the DSD and the second is a parameter of the DSD. Additional state variables increase the degrees of freedom of the retrieval, and require more information from observational variables to constrain the retrieval. Therefore we retrieve a single value of  $N_w$  for each profile, with the physical  
15 interpretation of representing  $N_w$  as constant with height, or as the vertically-averaged value. The representation of  $N_w$  as constant with height is not expected to be borne out in cases where evaporation or collision-coalescence processes modify the drop number concentration through the vertical profile. We take as the prior  $N_w$  the number concentration intercept of the Marshall and Palmer (1948) DSD,  $8 \times 10^6 \text{ m}^{-4}$ . ~~and assume  $N_w$  is constant with height in each profile.~~

When few observational variables are available, a single-parameter retrieval of  $R$  can be made by assuming that  $N_w$  is  
20 constant and equal to its prior holding  $N_w$  constant, reducing the degrees of freedom so that  $R$  is a function of  $D_0$  alone. This is called the “ $R$ -only” retrieval, and is similar to CloudSat rain rate retrievals in which  $N_w$  is assumed constant everywhere. When additional observational variables are available, such as the mean Doppler velocity, there may be sufficient information to also retrieve  $N_w$ ; this is called the  $R$ - $N_w$  retrieval.

We use the natural logarithms of  $R$  and  $N_w$  as the state variables, with the effect to ensure that the values remain positive  
25 everywhere and that the algorithm converges in fewer iterations faster. While in moderate stratiform rain  $R$  is often close to invariant with height (e.g. Matrosov, 2007), processes such as evaporation in the lower atmosphere and collision-coalescence in warm clouds will lead to significant variation with height in many contexts.  $R$  is therefore represented as the coefficients of a cubic spline basis function with  $n$  elements (Hogan, 2007); this has the effect of ensuring the vertical profile of  $R$  is smoothly varying and continuous with height, and also reducing the number of terms in the state vector. Table 1 summarises the rain  
30 state variables, their prior values and uncertainties, and physical representation constraints applied to their representation in each vertical profile. For  $R$ -only retrievals the state vector  $\mathbf{x}$  for a vertical profile with  $n$  elements, or pixels, is given by

$$\mathbf{x} = \ln \left[ R_1 \cdots R_n \right]^T \quad (4)$$

while for the  $R$ - $N_w$  retrieval the full state vector is

$$\mathbf{x} = \ln \begin{bmatrix} R_1 \cdots R_n & N_w \end{bmatrix}^T \quad (5)$$

where  $N_w$  is assumed constant with height in each profile. a single  $N_w$  is retrieved per profile. At moderate rain rates, we expect  $R$  to be close to invariant with height due to high fallspeeds and negligible evaporation (e.g. Matrosov et al. 2007; however, at low rain rates  $R$  may vary vertically, either due to evaporation in the lower atmosphere, or collision-coalescence processes in warm rain (Lebsock 2011)). Therefore to reduce noise and ensure smoothly varying rain rate with height, we retrieve each profile of  $R$  as the coefficients of cubic spline basis functions.

**Table 1.** Rain state variables  $\mathbf{x}_i$ , their prior values  $\mathbf{x}_i^a$  and uncertainties  $\sigma(\mathbf{x}_i^a)$ . The profile of rain rate  $R$  is always retrieved in each profile, while the drop number concentration parameter  $N_w$  may be either retrieved or assumed equal to the prior; the melting layer thickness scaling  $X_m$  is not retrieved in this study.

| $\mathbf{x}_i$ | $\mathbf{x}_i^a$                    | $\sigma(\mathbf{x}_i^a)$ | Vertical representation   |
|----------------|-------------------------------------|--------------------------|---|
| $\ln R$        | $\ln(0.1 \text{ mm h}^{-1})$        | 4.0                      | Retrieved as the coefficients of a cubic spline basis function, with a spacing of 300 m.    |
| $\ln N_w$      | $\ln(8 \times 10^6 \text{ m}^{-4})$ | 3.0                      | Retrieved as constant with height ( $R$ - $N_w$ retrievals), or not retrieved ( $R$ -only). |
| $X_m$          | 1.0 km                              | 0.0                      | Not retrieved in this study.  |

### 2.3.4 Stratiform precipitation melting layer

We employ a simplified representation of the melting layer in stratiform precipitation by applying radar attenuation between the lowest pixel in each profile classified as ice, and the highest pixel classified as rain, provided the two pixels are contiguous. Melting of graupel and hail, usually associated with convective precipitation, are not considered in this melting layer model. Following Matrosov (2008) Matrosov (2008), it is assumed that the two-way attenuation of the melting layer  $A$  is proportional to the rain rate  $R$  at the first pixel just below the melting layer, and the two-way path length  $X_m$  through the melting layer, such that

$$A = k_m X_m R \quad [\text{dB}] \quad (6)$$

where the melting layer extinction coefficient  $k_m$  is  $2.2 \text{ dB km}^{-1} (\text{mm h}^{-1})^{-1}$  at 94 GHz and  $0.04 \text{ dB km}^{-1} (\text{mm h}^{-1})^{-1}$  at 9.6 GHz. The estimated attenuation through the melting layer is based on a Marshall–Palmer DSD for the rain below the melting layer (Matrosov, 2008), and is not modified to match the retrieved DSD in the profile (Matrosov 2008). The thickness of the melting layer, and therefore the total attenuation, may also depend on the local temperature profile: as sufficient information to retrieve the total melting-layer attenuation may be available from the PIA and the attenuation inferred from the radar reflectivity gradient, we include the variable  $X_m$  in the retrieval to represent the effect of melting layer thickness on radar attenuation;

however, in this study ~~the~~  $X_m$  is held constant with a value of  $1.0 \text{ km}^4$ , allowing us to capture the effect of this uncertainty on the retrieved variables and their errors, without retrieving  $X_m$ .

### 2.3.5 Radar forward model

For a given state vector we estimate the corresponding measurements made by each instrument by forward modelling the  
 5 scattering behaviour between the sensor and each gate ~~for 94 GHz and 9.6 GHz radars~~, accounting for the effects of atmospheric gases, aerosols and hydrometeors.

The radar reflectivity factor of rain is a function of the sixth moment of the DSD,

$$Z = \int_0^{\infty} N(D) D^6 \gamma_f(D) dD \quad [\text{dBZ}], \quad (7)$$

where  $\gamma_f$  is the Mie–Rayleigh backscatter ratio at the radar frequency  $f$ , and is required for both 94 GHz and 9.6 GHz radars  
 10 to account for non-Rayleigh scattering ~~as drop sizes approach the radar wavelength~~. At 94 GHz the uncertainty of assuming raindrops are spherical Mie scatters is approximately 5% in integrated backscatter for a gamma DSD with median drop size  $D_0 = 1.5 \text{ mm}$ , when compared against estimates for oblate spheroids (e.g. Thurai et al., 2007; Zhang et al., 2001) using the T-matrix method (Mishchenko et al., 1996).

Scattering and attenuation effects are included in the radar forward-model ~~All major scattering effects are modelled~~, so that  
 15 the forward-modelled estimate of the apparent radar reflectivity ( $Z_a$ ) is directly comparable to observations. Attenuation due to atmospheric gases and the dielectric factor of water are calculated from atmospheric temperature and humidity profiles (Liebe, 1985). Multiple scattering effects ~~on radar and lidar backscatter can be estimated within CAPTIVATE for radar and lidar instruments can be estimated~~ using Hogan (2008). Radar reflectivity enhancement due to multiple scattering is especially relevant to spaceborne radar measurements at millimeter wavelengths (Battaglia et al., 2005), and the effects on Doppler radar  
 20 measurements are expected to include both enhanced spectral broadening and modified mean Doppler velocity (Battaglia and Tanelli, 2011); however, with the narrower beam of the airborne radar used in this study we can assume multiple scattering effects are negligible (Battaglia et al., 2007). ~~however for the aircraft measurements used in this study we assume multiple scattering effects are negligible.~~

Radar attenuation due to hydrometeors is quantified at each gate by the extinction coefficient

$$25 \quad k = \frac{\pi}{4} \int_0^{\infty} Q(D) N(D) D^2 dD \quad [\text{m}^{-1}] \quad (8)$$

where  $Q(D)$  is the extinction efficiency calculated from Mie theory (Mie, 1908). ~~As for radar reflectivity, the uncertainty in extinction due to assuming spherical drops is less than 2% for DSD with  $D_0$  of 1.5 mm.~~ The gradient of extinction can be related to the gradient of apparent radar reflectivity and used to estimate the rain rate as suggested by Matrosov (2007). A second approach to quantifying attenuation due to hydrometeors is to measure the two-way path-integrated attenuation

$$30 \quad \text{PIA} = 2 \frac{10}{\ln 10} \int_0^{\infty} k dz \quad [\text{dB}] \quad (9)$$

for each profile. PIA is estimated from the radar reflectivity at the ocean surface, and used as an observational measurement. Both approaches are implemented simultaneously, ~~so that~~; whereas the gradient method of Matrosov (2007) ~~is applied only at moderate to heavy rain rates, where it can be assumed that the gradient of apparent radar reflectivity is dominated by attenuation~~~~required an assumption of constant rain rate with height~~, within the CAPTIVATE variational scheme the gradient of

5  $R$  and  $k$  can be estimated simultaneously from the profile of radar reflectivity and the PIA.

Finally the mean Doppler velocity is the reflectivity-weighted mean drop fallspeed,

$$\bar{v}_D = \frac{-\int_0^\infty N(D)D^6v(D)\gamma_f(D) dD}{\int_0^\infty N(D)D^6\gamma_f(D) dD} \quad [\text{ms}^{-1}] \quad (10)$$

where the terminal fallspeed of drops  $v(D)$  is from the empirical formulation of Beard (1976) ~~scaled to account for air density changes with altitude~~~~corrected for air density~~, and where positive velocities are toward the ground. The forward-modelled mean

10 Doppler velocity is calculated assuming zero vertical air motion; therefore the difference between the forward-modelled and observed mean Doppler velocities will include a contribution from the vertical air motion, which is treated as an observational uncertainty.

The observed variables, their observational uncertainties and their vertical representation are summarized in Table 2. The ~~uncertainties in the observational variables include both estimated uncertainties in the measurements are relaxed somewhat from~~

15 the specified ~~measurement errors~~~~uncertainties~~ for the CRS instrument (Li et al., 2004) ~~and the estimated uncertainties in the radar forward model~~, ~~so that the uncertainty in radar reflectivity is taken as 3 dB, and as 1.0 ms<sup>-1</sup> 0.5 ms<sup>-1</sup> for mean Doppler velocity~~. We have found that the weighting of errors between radar reflectivity and PIA is quite important for the retrieved rain rate, and that if only instrument errors are included the retrieval is not sufficiently constrained by PIA. This is believed to be because attenuation affects all forward-modelled radar reflectivity measurements in the same way, leading to them having

20 strong error correlations. Error correlations are not accounted for in the  $\mathbf{R}$  matrix, since they are profile-dependent and difficult to estimate, which can lead to the radar reflectivity measurements being over-weighted in the retrieval. To overcome this, we take the common approach (e.g. Weston et al., 2014) of inflating the reflectivity errors (and in our case somewhat reducing the errors in PIA) to better balance the information coming from the reflectivity profile and from PIA.

**Table 2.** Observational variables  $y_i$  for Doppler radar, and their estimated uncertainties  $\sigma(y_i)$  as used in the retrieval. Apparent radar reflectivity  $Z_a$  and mean Doppler velocity  $\bar{v}_D$  are measured at each gate, while PIA is estimated from the radar reflectivity over the ocean surface.

| $y_i$       | $\sigma(y_i)$        | Vertical representation     |
|-------------|----------------------|-----------------------------|
| $Z_a$       | 3.0 dB               | At each radar gate          |
| $\bar{v}_D$ | 1.0 ms <sup>-1</sup> | At each radar gate          |
| PIA         | 0.5 dB               | Integrated for each profile |

### 3 Retrievals of rain rate with attenuated radar

The strong attenuation of 94 GHz radar by ~~liquid water, and especially by~~ rain, presents a challenge for retrievals of rain rate from profiles of ~~apparent~~ radar reflectivity (Hitschfeld and Bordan, 1954). For nadir-pointing radars the following ambiguity arises: when the profile of apparent radar reflectivity decreases with range (toward the ground), the decrease could be due to either the attenuation of the radar beam, or to a physical change in the rain DSD (e.g., due to evaporation). These two possibilities each constitute a local minimum in the cost function, so that a profile of evaporating light rain with negligible attenuation may be wrongly identified as a profile of moderate rain with significant attenuation, and visa versa.

To illustrate the double-minimum problem, and to visualise how PIA and Doppler velocity may help resolve this retrieval ambiguity, we use the radar forward model to generate synthetic radar measurements assuming zero observational noise. In practice, measurement error and more complex profiles will introduce further uncertainties in the retrieval than in this synthetic case. Two synthetic profiles of rain are simulated, with constant rain rates of  $0.05 \text{ mm h}^{-1}$  and  $5.0 \text{ mm h}^{-1}$  below a level of 5 km, and drop number concentration  $N_w = 8 \times 10^6 \text{ m}^{-4}$ , representing a profile of light rain with negligible attenuation, and of moderate rain with strong attenuation, respectively. In making the inverse retrieval of the profile of rain rate corresponding to a given profile of 94 GHz radar reflectivity, multiple solutions may be found depending on the prior rain rate: the low- $R$  and high- $R$  profile of  $R$  (Fig. 1a) represent the two minima of the cost function for the retrieval from the radar reflectivity profile (Figs. 1b) corresponding to the  $5.0 \text{ mm h}^{-1}$  profile of rain (the “truth”). The radar reflectivity alone does not provide sufficient information to differentiate between the two solutions; however, the forward-modelled mean Doppler velocity profile (Fig. 1c) and PIA (Fig. 1d) for the two solutions illustrate how additional observational variables may provide further information with which to resolve the ambiguity. The PIA differs by more than 30 dB between the two solutions, and is used effectively to differentiate light and moderate rain in CloudSat rain retrievals. The mean Doppler velocity profiles also differ significantly, with the “true” high- $R$  profile varying only slightly with altitude, while the gradient of mean Doppler velocity indicates a reduction of  $D_0$  toward the surface in the low- $R$  profile. An additional advantage of the mean Doppler velocity is that it is not affected by the partial attenuation of the radar.

We can quantify the contribution of the observational variables to resolving ambiguous retrievals using the cost function that is minimized within the variational retrieval scheme. A range of prior rain rates are taken as candidates for the starting-point of the retrieval, and for each prior  $R$  the contribution of the observations to the cost function is calculated by

$$J_{\text{obs}} = \frac{1}{2} \sum \frac{(\mathbf{y}^f - \mathbf{y})^2}{\sigma_{\mathbf{y}}^2}. \quad (11)$$

which is equivalent to the first term of the cost function in equation (1). We can interpret the curve of  $J_{\text{obs}}$  (Fig. 1e) as showing the tendency of the retrieval algorithm to converge from any prior  $R$  toward a local minimum in the cost function, wherein a steeper curve indicates stronger convergence toward a more robust retrieval. To explore the contributions of the observational measurements, we run the retrievals for the two synthetic profiles with only radar reflectivity observations (“Z-only”), with one additional observational variable (“ZPIA”, “Zv”), and with all available observations (“ZvPIA”).

For the light rain profile, the cost function for the Z-only retrieval has a secondary minimum at  $3.0\text{--}4.0\text{ mm h}^{-1}$ . The bimodal shape of  $J$  shows that the retrieval is sensitive to the choice of prior: if  $R$  is less than  $1.0\text{ mm h}^{-1}$ , the retrieval will converge to the “true”  $R$  profile, but if the prior  $R$  is greater than  $1.0\text{ mm h}^{-1}$  the retrieval will converge on the high- $R$  solution. Conversely, for the moderate rain profile, the Z-only retrieval will converge on a low- $R$  solution if the prior is less than around  
5  $0.5\text{ mm h}^{-1}$ . These two solutions are compared in Figs. 1a–1d.

The effect of including PIA (dashed lines in Fig. 1e) is strongest for  $R > 1.0\text{ mm h}^{-1}$ , and this removes any sensitivity to the prior  $R$ , while the effect of including Doppler velocity (darker lines in Fig. 1e) is smoother across the full range of  $R$  than that of PIA, and dominates at low  $R$  where radar attenuation is negligible. When both PIA and Doppler measurements are used the effects are cumulative, and the gradient of  $J$  shows even stronger convergence toward the unique solution.

10 This example provides a simple illustration of the bimodal cost function of an  $R$ -only rain retrieval with a strongly attenuating 94 GHz radar. Without additional observational measurements, a given profile of radar reflectivity may equally be explained by a strongly attenuating profile with constant  $R$ , or by a weakly attenuating profile in which  $R$  decreases toward the surface. Either PIA or mean Doppler velocity are sufficient to resolve this ambiguity: PIA as a constraint on the total attenuation, and mean Doppler velocity on the profile of  $D_0$ . As PIA is typically estimated from the ocean surface backscatter, the availability  
15 of mean Doppler velocity to resolve these ambiguities presents an opportunity for Doppler radar estimates of rain rate over land.

#### 4 Retrievals of rain rate and drop number concentration

We now ~~combineput to use observations of both~~ PIA and mean Doppler velocity, in addition to radar reflectivity, to make  $R$ - $N_w$  rain retrievals from 94 GHz Doppler radar measurements. Three cases of stratiform rain are selected from two ER-2  
20 flights during TC4 (Fig. 2): two flight legs on 22 July 2007 include rain falling from melting ice, ranging in intensity from virga to heavy showers, and a case of light to moderate warm rain from liquid clouds is observed on 29 July 2007.

For each case the  $R$ - $N_w$  retrieval is performed using all available measurements from the 94 GHz radar: radar reflectivity, mean Doppler velocity and PIA. This “ZvPIA” retrieval is of primary interest for evaluating the full capabilities of the CAPTIVATE retrieval for a Doppler cloud radar; however, we are also interested in the capabilities of a retrieval when one  
25 of the observational measurements is not available, or has high observational uncertainty. When mean Doppler velocity measurements are not used (ZPIA), the observational variables are analogous to those available to CloudSat over ocean; however, unlike CloudSat rain retrievals, here we retrieve  $N_w$  as well as  $R$ . Conversely, when PIA is not used (Zv) the observational variables are similar to those available to a Doppler radar over land, where the land surface cannot be sufficiently characterised to estimate PIA. The ZPIA and Zv retrievals of  $R$ - $N_w$  are less constrained by observations than the ZvPIA retrieval, and will  
30 therefore demonstrate some bimodal or poorly constrained retrievals similar to those demonstrated for  $R$ -only retrievals in Section 3; nevertheless, we include ZPIA and Zv retrievals in order to demonstrate the information provided by the PIA and mean Doppler velocity separately, and to identify situations in which a satisfactory  $R$ - $N_w$  retrieval may be made with limited observational variables.

In each case the retrieval is evaluated by forward-modelling all 94 GHz and 9.6 GHz radar variables, whether or not they were assimilated in the retrieval, and comparing against the observations. ~~In each case the retrievals are evaluated by forward-modelling independent radar measurements at the unattenuated frequency, and comparing the retrievals at a selected height above sea level.~~

#### 5 4.1 Case 1: moderate rain from melting ice, 22 July 2007

Stratiform rain from melting ice provides a test of many of the simplifying assumptions made in rain retrievals. At moderate and heavy rain rates we expect  $R$  to be close to constant with height, unless significant evaporation is evident (Haynes et al., 2009).  $N_w$  may be expected to be close to values deemed typical by Marshall and Palmer (1948) or Testud et al. (2001), i.e. between  $2.0 \times 10^6 - 8.0 \times 10^6 \text{ m}^{-4}$ , and constant with height (Tokay and Short, 1996). From in situ measurements of stratiform rain we expect median drop sizes ~~in this case~~ to be in the range 1.0–1.5 mm (Tokay and Short, 1996).

Between 15:54 and 16:03 UTC on 22 July 2007 ER-2 overflew approximately 110 km of ~~precipitating stratiform cloud~~ ~~stratiform precipitation~~ around 50 km south of the coast of Panama (Fig. 2). Radar, lidar and radiometer measurements (Fig. 3) reveal distinct regimes of light, moderate and heavy rain below a melting layer around 4.5 km above sea level, contiguous with ice clouds with tops between 6–10 km. The scene is overlain by cirrus between 10–15 km, ~~which is primarily detected by the lidar~~. In light rain between 15:54 and 15:55 UTC the 94 GHz radar is barely attenuated. Moderate stratiform rain follows from 15:55 and 16:03 UTC, with a strong 9.6 GHz bright band ~~evident~~, and 94 GHz PIA between 5 and 20 dB. Finally a heavy shower is embedded within the moderate rain between 16:01 and 16:02 UTC. In the latter regime the 94 GHz radar is completely attenuated such that PIA saturates around ~~60 dB~~ ~~65 dB~~; 94 GHz radar reflectivity and mean Doppler velocity measurements are therefore not available within ~~these~~ ~~the~~ heaviest rain profiles.

The retrieved variables (Figs. 4a–4e), and forward-modelled 94 GHz and 9.6 GHz radar measurements (Figs. 4f–4j) are compared for the ZvPIA, Zv and ZPIA retrievals. We evaluate the retrievals at a height of 3 km above sea level, approximately 1 km below the melting layer.

##### 4.1.1 Moderate rain (15:55–16:01 and 16:02–16:03 UTC)

In the moderate rain regime the ZvPIA retrieval estimates rain rates of  $1.0 - 2.0 \text{ mm h}^{-1}$  at the melting layer. In profiles with strong attenuation (PIA up to 20 dB),  $R$  is ~~close to~~ constant from the melting layer to the surface; conversely, in less attenuated profiles (with PIA around 10 dB) ~~some~~ evaporation is evident, with  $R$  reducing to  $0.1 - 1.0 \text{ mm h}^{-1}$  at the surface (Fig. 4a). Estimates of  $N_w$  are consistently between  $10^6 - 10^7 \text{ m}^{-4}$  in this regime (Fig. 4c), close to the Marshall and Palmer (1948) value, ~~while~~;  $D_0$  is around 1.0 mm at the melting layer ~~and decreases,~~ ~~reducing~~ somewhat toward the surface in profiles where evaporation is strong (Fig. 4d). Forward-modelled 94 GHz radar measurements agree with observations at 3 km (Figs. 4f–h), as expected since the retrieval minimizes differences between the observed and forward-modelled variables. ~~Comparisons of the independent~~ 9.6 GHz radar measurements ~~with those~~ forward-modelled from the retrieved state show ~~generally~~ good agreement ~~with independent observations~~ at 3 km above sea level (Figs. 4i and 4j), although 9.6 GHz radar reflectivity is overestimated by as much as 3 dB in profiles with strong evaporation between 15:58 and 16:00 UTC, ~~and mean Doppler velocity is under-~~

estimated in the profiles with the heaviest rain. ~~Moderate rain profiles with significant evaporation are well represented by the ZvPIA retrieval, however these profiles correspond to the strongest differences compared to the independent 9.6 GHz radar reflectivity.~~

The averaged vertical profiles of the ZvPIA retrieval in moderate rain (Fig. 5), show that the forward-modelled 94 GHz radar reflectivity is over-estimated near the surface, while the largest error in 9.6 GHz is in the mean Doppler velocity in the lowest 2–3 km. We suggest that these errors in the forward-modelled variables through the vertical profile relate to the representation of  $N_w$  as constant with height, such that the effects of evaporation on the DSD—a decrease in concentration of the smallest drops—is not resolved. In a vertically-averaged sense, however, the ZvPIA retrieval is broadly able to reproduce the 9.6 GHz radar reflectivity, while slightly under-estimating mean Doppler velocity.

~~We use the~~The ZPIA and Zv retrievals ~~of  $R$  and  $N_w$  illustrate to demonstrate~~ the contributions of mean Doppler velocity and PIA to a ~~ZvPIA successful~~ retrieval, and the ambiguities that arise in under-constrained retrievals. Both ZPIA and Zv retrievals are considerably more sensitive to the selection of priors ~~and uncertainties~~ than the ZvPIA retrieval. At 3 km above sea level (Fig. 4), ZPIA estimates of  $R$  in the moderate rain regime are close to those of ZvPIA, but  $N_w$  and  $D_0$  differ significantly, with ZPIA estimating a much higher concentration of smaller drops than ZvPIA. Forward-modelled mean Doppler velocity shows that this retrieval leads to ~~large significant~~ errors in ~~of~~ drop fallspeeds. The Zv retrieval ~~tends to underestimate~~underestimates the rain rate in this regime by up to an order of magnitude, tending toward the prior  $R$  of  $0.1 \text{ mm h}^{-1}$ , with the exception of the strongly attenuated profiles 15:57–15:58 UTC where Zv is able to reproduce the observed PIA from the profiles of radar reflectivity and mean Doppler velocity: while  $D_0$  is well constrained by the mean Doppler velocity, without a constraint on PIA ~~the total attenuation from PIA~~; the retrieved drop number concentration ~~and rain rate are~~ lower than that estimated from ZvPIA; the forward-modelled observations confirms that the Zv retrieval meets reflectivity and mean Doppler velocity constraints, but tends to ~~toward~~representing weakly-attenuating profiles of rain; the forward-modelled 9.6 GHz ~~variables measurements~~ show that this retrieval leads to a significantly under-estimated ~~in~~ radar reflectivity at this frequency ~~the unattenuated wavelength~~.

~~Selected profiles of retrieved and forward-modelled variables at 15:58:00 UTC (Fig. 5) illustrate how the Zv and ZPIA retrievals differ from ZvPIA through the vertical profile. With constraints on PIA, both ZPIA and ZvPIA retrievals estimate profiles of  $R$  that are close to constant with height; without a Doppler constraint on drop size, the ZPIA retrieval represents the observed PIA with a higher number of smaller drops than the ZvPIA retrieval, leading to a mean Doppler velocity around  $1.0 \text{ m s}^{-1}$  lower than observed. Conversely, the Zv retrieval has a strong constraint on drop size and therefore forward-modelled mean Doppler velocity, but without a constraint on PIA  $N_w$  is underestimated a low concentration of drops is estimated, with  $R$  and  $D_0$  decreasing toward the surface.~~

#### 4.1.2 Light rain (15:54–15:55 UTC)

In the light rain regime, ZvPIA estimates  $R$  in the range  $0.002$ – $0.1 \text{ mm h}^{-1}$  and  $N_w$  in the range  $10^5$ – $10^6 \text{ m}^{-4}$ . The lower rain rate corresponds to an observed  $1.0 \text{ m s}^{-1}$  decrease in 94 GHz mean Doppler velocity compared to the moderate rain regime; the retrieval resolves smaller drops in the light rain, with  $D_0$  around 0.5 mm. The forward-modelled 9.6 GHz radar measurements from the ZvPIA retrieval are consistent with independent observations.

$Z_v$  retrieves  $R$  consistent with  $Z_v$ PIA throughout the light rain regime, while  $Z$ PIA somewhat overestimates  $R$  in these profiles. PIA is negligible and therefore provides little additional information in this regime: therefore the  $Z$ PIA retrieval represents a higher concentration of smaller drops as the retrieved  $R$  and  $N_w$  tends to the priors. This sensitivity to the prior when observational information is limited was demonstrated in Section 3 and, as in that synthetic case, the  $Z$ PIA retrieval here could be improved with a more appropriate prior. In contrast, with Doppler velocity information to constraint drop size and PIA negligible, the DSD retrieved by  $Z_v$  is very close to that of  $Z_v$ PIA. The strong performance of  $Z_v$  in light rain suggests strong potential for using Doppler radar for  $R$ - $N_w$  retrievals of light rain over land.

#### 4.1.3 Heavy shower (16:01–16:02 UTC)

The upper limit of the 94 GHz radar frequency for rain retrievals is reached in the heavy shower, where PIA is saturated and no radar reflectivity or Doppler information is available below the melting layer. Based on the saturated PIA and the gradient of radar reflectivity in the first few gates, both  $Z_v$ PIA and  $Z$ PIA retrievals estimate  $R$  up to  $10 \text{ mm h}^{-1}$ ; large uncertainties in  $R$  reflect the dearth of information available for retrievals in these profiles, however the 9.6 GHz radar measurements are broadly consistent with profiles in which  $Z$ PIA and  $Z_v$ PIA estimate rain rates around  $10 \text{ mm h}^{-1}$ . Without PIA information, the  $Z_v$  retrieval interprets the deficit in radar reflectivity as a drop in rain rate and drop size, and adds significant uncertainty to the retrieved quantities. The estimates of  $N_w$  vary over many orders of magnitude and are clearly unconstrained by observations in this regime; the  $R$ - $N_w$  retrieval is not warranted without sufficient observational information, however PIA does appear to be sufficient for to estimate  $R$ , with increased uncertainty.

In this case of tropical stratiform rain the 94 GHz radar is fully attenuated by rain rates around  $10 \text{ mm h}^{-1}$  falling from a melting layer around 4.0 km above sea level. In the midlatitudes, however, where melting layers are much shallower, successful  $R$ - $N_w$  retrievals should be possible up to higher rain rates before the radar is fully attenuated.

#### 4.1.4 Joint frequencies of retrieved and forward-modelled variables

A more comprehensive evaluation of the retrievals against independent 9.6 GHz radar measurements can be made using the joint frequencies of retrieved state variables (Figs. 6a–6c) and forward-modelled 9.6 GHz radar measurements (Figs. 6d–6f) for each retrieval. The major modes in the rain retrieval are evident in the distributions of  $R$  and  $N_w$  relative to the priors (dashed lines), and in the distribution of 9.6 GHz radar reflectivity and mean Doppler velocity compared against observations (black contours). In the 9.6 GHz radar variables the moderate rain regime exhibits radar reflectivity around 20 dBZ and mean Doppler velocity between  $6$ – $7 \text{ ms}^{-1}$ , while the light rain regime has radar reflectivity between  $0$ – $5 \text{ dBZ}$  and mean Doppler velocity around  $3 \text{ ms}^{-1}$ .

The  $Z$ PIA retrieval has a dominant mode corresponding to the moderate rain regime, with  $R$  between  $0.5$ – $2.0 \text{ mm h}^{-1}$  and a higher  $N_w$  with respect to the prior; without a constraint on mean Doppler velocity this retrieval represents a relatively high concentration of small drops. The corresponding forward-modelled measurements shows the small drop size leads to a significant underestimate of both mean Doppler velocity and radar reflectivity at 9.6 GHz.

Without a PIA constraint,  $Z_v$  retrievals in the moderate rain regime tend toward weakly attenuated profiles with  $N_w$  less than  $10^6 \text{ m}^{-4}$ , where  $R$  is close to the prior. This leads to underestimates of radar reflectivity by more than 10 dB; the mean Doppler velocity is reasonably well-constrained, but broadly underestimated by around  $1 \text{ m s}^{-1}$ . A secondary mode with  $N_w$  close to the prior and  $R$  greater than  $1 \text{ mm h}^{-1}$  represents the strongly attenuated profiles of moderate rain in which  $Z_v$  comes close to reproducing the observed PIA. Light rain profiles are represented with  $N_w \approx 10^6 \text{ m}^{-4}$ , somewhat overestimating mean Doppler velocity.

$Z_v$  PIA resolves distinct modes for light and moderate rain regimes in the retrieved variables, and each mode corresponds well to the observed 9.6 GHz radar measurements: the moderate rain regime is represented with heavier rain than the  $Z_v$  retrieval, but with a lower concentration of smaller drops than the ZPIA retrieval; the light rain regime is similar to that of the  $Z_v$  retrieval, where the negligible PIA provides little additional information. Both rain regimes have  $N_w$  around  $10^6 \text{ m}^{-4}$ , consistent with the average value of  $2 \times 10^6 \text{ m}^{-4}$  for stratiform rain found by Testud et al. (2001). The 9.6 GHz radar reflectivity is well-represented across both rain regimes, however the mean Doppler velocity shows that drop fallspeed is slightly under-estimated in moderate rain, and over-estimated in the light rain; this may be due to the retrieval assuming  $N_w$  is constant with height in each profile, such that any variations in the DSD with height are expressed as changes in drop size, rather than in drop number concentration.

We have retrieved  $R$  as a function of both  $D_0$  and  $N_w$  for a case of stratiform rain from melting ice, including across rain rates varying from light rain as low as  $10^{-3} \text{ mm h}^{-1}$ , to a heavy shower with  $R$  up to  $10 \text{ mm h}^{-1}$ . The retrieved  $N_w$  was around  $10^6 \text{ m}^{-4}$  throughout the case, which is consistent with expectations for average drop number concentrations in this context; the exception is in the heavy rain shower where the 94 GHz radar becomes fully attenuated, and insufficient information is available for a  $R$ - $N_w$  retrieval. The  $Z_v$  retrieval, an analogue for Doppler radar retrievals over land, performed very well in light rain where total attenuation is close to zero, but tended towards the  $R$  prior in profiles of moderate rain where attenuation makes radar reflectivity ambiguous, and  $R$  tends to be under-estimated. ZPIA retrievals without mean Doppler velocity information tend to estimate  $R$  broadly accurately, but retrieve DSDs with a high number concentration of small drops, leading to errors with respect to the independent radar measurements; indeed, since the estimated  $N_w$  were close to expectations in this context, a good non-Doppler retrieval of  $R$  could have been made by assuming the value of  $N_w$  is equal to the prior.

#### 4.2 Case 2: evaporating rain from melting ice, 22 July 2007

We now evaluate the  $R$ - $N_w$  retrieval for a case of very light rain from melting ice, much of which evaporates before reaching the ground. ER-2 overflew a 60 km section of stratiform ice cloud 300 km south of Costa Rica, between 13:12:00–13:17:30 UTC on 22 July 2007. Light rain was observed below ice clouds with tops between 10–12 km (Fig. 7). Below the melting layer both 94 GHz and 9.6 GHz radar reflectivity are less than 10 dBZ and decreased toward the surface; the exception is a region of higher 9.6 GHz radar reflectivity between 13:16–13:17 UTC, and 94 GHz

PIA is small but non-negligible, around 3 dB. In combination with low 94 GHz PIA, the observations suggest significant evaporation stratiform light rain evaporating in the lower atmosphere, including significant virga.

Time series of retrieved variables (Figs. 8a and 8e), and forward-modelled 94 GHz and 9.6 GHz radar measurements (Figs. 8f and 8j) are evaluated against observations. We compare ZPIA,  $Z_v$  and  $Z_v$ PIA retrievals at a height of 4 km above sea level, which is just below the melting layer.

$Z_v$ PIA makes a consistent representation retrieval of evaporating light stratiform rain, with  $R$  between  $0.1-0.2 \text{ mm h}^{-1}$  at the melting layer, down to a minimum detectable rate of  $10^{-3} \text{ mm h}^{-1}$  near the surface or at the limits of the virga. In the heaviest rain profiles between 13:16–13:17,  $R$  is around  $0.1 \text{ mm h}^{-1}$  at the surface, with  $D_0$  as large as 1.5 mm. Retrieved  $N_w$  is consistently around  $10^5 \text{ m}^{-4}$ , an order of magnitude lower than the previous case of stratiform rain from melting ice, and significantly lower than the prior. Forward-modelled 9.6 GHz radar variables shows very good agreement with independent measurements 4 km; which can be expected as there should be little ambiguity in the retrieval due to attenuation; however, the averaged vertical profiles (Fig 9) show that, while the vertical profile of 94 GHz variables are well-represented, 9.6 GHz radar reflectivity is strongly underestimated in the lowest 3 km. We suggest that these errors in the vertical distribution are due to the effects of evaporation on the DSD, which are not fully resolved in this retrieval of  $N_w$  as constant with height: we would expect  $N_w$  to decrease toward the surface as the smallest drops evaporate, while errors in forward-modelled mean Doppler velocity at both radar frequencies suggest the raindrop size may be underestimated near the surface.

Similar to the light rain profiles of Case 1, both ZPIA and  $Z_v$  retrievals make estimates of  $R$  close to the  $Z_v$ PIA retrieval. ZPIA retrievals slightly overestimates  $R$  with  $N_w$  again close to the prior, which is 2 to 3 orders of magnitude higher than  $Z_v$ PIA estimates; the corresponding low  $D_0$  of around 0.5 mm leads to significant differences between forward-modelled and observed mean Doppler velocities.  $Z_v$  estimates of  $D_0$  are well-constrained by mean Doppler velocity, and where PIA is negligible the  $Z_v$  retrieval is identical to that of  $Z_v$ PIA. As noted in the previous case, this indicates that it may should be possible to make an accurate  $R$ - $N_w$  retrieval of light rain over land with Doppler radar.

### 4.3 Case 3: warm rain from liquid clouds, 29 July 2007

In warm rain from liquid clouds we expect a distinct DSD with a higher concentration of smaller drops, and with drop growth between cloud-top and the surface (Lebsock et al., 2011). On 29 July 2007 ER-2 overflew a 120 km section of precipitating warm marine cloud around 500 km south of Costa Rica between 12:41–12:51 UTC (Fig. 10). In the first part of the flight (12:41–12:46 UTC) observations suggest moderate rainfall corresponding to deeper cloud tops around 3.5 km: PIA varies between 10–50 dB in narrow features, where 9.6 GHz radar reflectivity exceeds 20 dBZ. The following section (12:46–12:51 UTC) is characterised by shallower stratiform cloud with tops around 3 km, and is associated with patchy light precipitation and with PIA between 0–10 dB.

Concurrent to the rain retrieval shown here, we use the lidar to retrieve liquid cloud, which also contributes to the attenuation of 94 GHz radar. The retrieved properties of the liquid cloud do not vary between the different retrievals compared here, and we do not evaluate the retrieval of cloud liquid water content in this study; however, as discussed in Section 2.2, lidar is quickly extinguished at cloud-top and radar is most sensitive to drizzle drops, so that cloud base is rarely known in the target

classification. Hence we acknowledge that the simultaneous retrieval of cloud and precipitation in warm clouds from 94 GHz radar is a source of uncertainty that warrants further consideration (e.g. Haynes et al., 2009; Hawkness-Smith, 2010; Mace et al., 2016).

The retrieved variables (Fig. 11a–11e) and forward-modelled radar measurements (Fig. 11f–11j) are compared at 1 km above sea level, and compared against 94 GHz and 9.6 GHz radar measurements. We compare ZPIA,  $Z_v$  and  $Z_v$ PIA retrievals as in the previous cases. Warm rain or drizzle forming from collision and coalescence in liquid clouds can be easily distinguished from rain falling below ice clouds within the target classification scheme, so that physically appropriate choices for the priors and the physical representations of state variables can be configured in CAPTIVATE for distinct warm and “cold” rain regimes; however, in this study we use the same prior  $R$  and  $N_w$  throughout.

### 4.3.1 Moderate rain (12:41–12:46 UTC)

The  $Z_v$ PIA retrieval resolves a strong increase in rain rate from cloud-top, where  $R$  is between  $0.1–1.0 \text{ mm h}^{-1}$ , to the surface, where  $R$  increases to  $1.0–10.0 \text{ mm h}^{-1}$ . Retrieved  $N_w$  is consistently around  $10^{10} \text{ m}^{-4}$  in the moderate rain regime, several orders of magnitude greater than were estimated for rain from melting ice; accordingly, the drop sizes are much smaller, with  $D_0$  increasing from  $0.1–0.3 \text{ mm}$  at cloud-top, to  $0.2–0.5 \text{ mm}$  near the surface. At 1 km above sea level the 94 GHz radar measurements correspond very well to the forward-modelled variables, and the 9.6 GHz radar reflectivity is also exceptionally close to the forward-model; this is because at the small drop sizes in this context scattering is in the Rayleigh regime for both radar frequencies; however, while the forward-modelled mean Doppler velocity at 9.6 GHz also tracks well with observations, peaks associated with the heaviest precipitation features are not resolved.

The vertical structure of 94 GHz and 9.6 GHz radar reflectivity is well represented in the  $Z_v$ PIA retrieval over the moderate warm rain regime (Fig 12); however, mean Doppler velocity is under-estimated by around  $1 \text{ m s}^{-1}$  in the lowest 1 km at both radar frequencies. The retrieval of constant- $N_w$  for each profile allows a broadly satisfactory retrieval of the rain DSD with a good fit to observations, but evaluation of the full vertical profiles shows that some microphysical process is not resolved: in warm rain we expect collision and coalescence to lead to both an increase in drop size and a decrease in drop number concentration toward the surface. It seems likely, as for the representation of evaporation in case 2, that while the retrieval of  $N_w$  allows for an improved retrieval of the DSD across a range of rain regimes, there are limits to the vertical variability of the DSD that can be resolved with a height-invariant  $N_w$ .

At 1 km the ZPIA retrieval closely resembles  $Z_v$ PIA; this includes matching estimates of  $D_0$ , despite having no constraint on drop size from mean Doppler velocity. The forward-modelled 94 GHz and 9.6 GHz mean Doppler velocities for the ZPIA retrieval are very close to observations.  $Z_v$  retrieves similar  $D_0$ . In contrast,  $Z_v$  also retrieves  $D_0$  correctly, but frequently under-estimates  $N_w$  by as much as 2 orders of magnitude: the  $Z_v$ -retrieved DSD has fewer drops and negligible PIA at 94 GHz, which corresponds to very large errors in forward-modelled 9.6 GHz radar reflectivity. Unlike the stratiform rain cases, here PIA is more important for an accurate retrieval than mean Doppler velocity: the mean Doppler velocity is less sensitive to the changes in terminal fallspeed due to variations in the sizes of small drops, while PIA in combination

with radar reflectivity provide an effective constraint on the number concentration because only a DSD with many small drops satisfies the observed strong attenuation and low radar reflectivity.

### 4.3.2 Light rain (12:46–12:51 UTC)

In the light warm rain ZvPIA estimates patchy precipitation features with  $R$  between  $0.01 - 0.5 \text{ mm h}^{-1}$  and median drop sizes around  $0.1 - 0.3 \text{ mm h}^{-1}$ , similar to values at the tops of the deeper warm clouds, but without significant drop growth toward the surface. The retrieved  $N_w$  in the lightest rain profiles is around  $10^8 - 10^9 \text{ m}^{-4}$ , but returns to  $10^{10} \text{ m}^{-4}$  where heavier rain features are evident. The forward-modelled radar reflectivities are close to observations at 1 km, while the mean Doppler velocity again matches the lower range of measurements, but not the noisy peaks. ~~The forward-modelled PIA is 0 dB in the lightest rain profiles, while measurements indicate non-zero attenuation of around 1–3 dB.~~ ZPIA estimates  $R$  similar to ZvPIA in the stratus regime, but without a Doppler velocity constraint in the lightest profiles, ZPIA retrieves fewer, larger drops, with  $N_w$  tending toward the prior at  $8 \times 10^6 \text{ m}^{-4}$ . In contrast, Zv is very similar to ZvPIA in the lightest profiles-rain.

~~In warm rain, we have retrieved~~  
~~In summary, it is possible to retrieve  $N_w$  several orders of magnitude greater than the Marshall–Palmer value, with  $D_0$  in the range  $0.1 - 0.5 \text{ mm}$  in rain rates across a range of  $R$  from very light drizzle, up to  $10 \text{ mm h}^{-1}$  in the heaviest profiles of warm rain from liquid clouds.~~ The contribution of PIA and mean Doppler velocity to  $R$ - $N_w$  retrievals in warm rain differs from that in rain from melting ice: while Doppler is required to retrieve  $N_w$  when attenuation is low, it is possible to retrieve  $N_w$  without Doppler in strongly attenuated profiles of warm cloud, where the combination of low radar reflectivity and high attenuation can only be due to a high concentration of small drops.

## 5 Dual-frequency radar retrievals

ER-2 aircraft measurements from TC4 provide a rare opportunity for airborne observations with multiple Doppler radars. In this study we have primarily used the 9.6 GHz radar to evaluate retrievals made with the 94 GHz radar; however, we can also use the dual-frequency radar measurements to exploit the different scattering behaviours and retrieve additional information about the DSD. Dual-frequency ratio (DFR) and differential Doppler velocity (DDV) techniques have been applied to retrievals from ER-2 measurements during the CRYSTAL-FACE field experiment over Florida in 2002 (Liao et al., 2008, 2009), and Tian et al. (2007) exploited dual-frequency Doppler radar to retrieve rain DSD and vertical air motion for light stratiform rain from the same experiment. The CAPTIVATE framework can combine information from two radars, resolving differential non-Rayleigh scattering and mean Doppler velocities from multiple wavelengths.

~~We compare the~~ The dual-frequency radar retrievals, with and without mean Doppler velocity measurements, are compared against the ZvPIA 94 GHz retrieval for Case 1 on 22 July 2007, which covered a wide range of rain intensities, including a region in which the 94 GHz radar was fully attenuated (Fig. 13). The dual-frequency radar retrieval estimates of  $R$  are consistent with those from 94 GHz retrievals, with the exception of the non-Doppler dual-frequency radar retrieval in the light rain, where

a high concentration of small drops is estimated, leading to an over-estimate of  $R$ ; in much of the lightest rain profiles the hydrometeors may be below the sensitivity of the 9.6 GHz instrument, so that the dual-frequency radar retrieval tends toward that of the ZPIA retrieval from the 94 GHz radar. In the heavy shower, where the ZvPIA estimates of  $Z$  have large uncertainties and  $N_w$  is very poorly constrained due to complete extinction of the 94 GHz radar beam, the dual-frequency radar retrievals use the unattenuated 9.6 GHz measurements alone to estimate  $R$  around  $10 \text{ mm h}^{-1}$ ;  $N_w$  remains in the range  $10^6 - 10^7 \text{ m}^{-4}$  as in the surrounding moderate rain, and  $D_0$  is estimated between 1–2 mm. This illustrates and confirms that the 94 GHz retrieval was capable of a cautious estimate of  $R$  with large retrieval uncertainty, based on the gradient of radar reflectivity and saturated PIA; however, ZvPIA estimates of  $N_w$  cannot be justified when the radar is fully attenuated. The greatest errors in the non-Doppler dual-frequency radar retrieval are in forward-modelled Doppler velocity for the evaporating moderate rain profiles between 15:58–16:00 UTC, where a higher concentration of smaller drops is retrieved; in this circumstance the addition of Doppler velocity information leads to a stronger retrieval than a second radar wavelength. Overall the close agreement of the 94 GHz Doppler radar retrievals with the dual-frequency Doppler retrieval is a promising result, indicating that a single frequency Doppler radar is sufficient for a retrieval of  $R$  and  $N_w$  within the limits of radar attenuation.

## 6 Retrieving vertical profiles of $N_w$

We have demonstrated the retrieval of rain rate as a function of both  $D_0$  and  $N_w$ , making the simplifying assumption that  $N_w$  is constant with height in each profile. We argue that this is a significant improvement over retrievals in which  $N_w$  is assumed constant everywhere, and have retrieved values of  $N_w$  ranging over more than five orders of magnitude between light rain from melting ice and warm rain from liquid clouds; however, evaluation against 9.6 GHz radar measurements showed that features within the vertical profile are not always accurately resolved, with the most significant errors near the surface in cases where microphysical processes are expected to affect the DSD with height.

It is of interest to represent changes in  $N_w$  through the vertical profile; however, there are limits to the degrees of freedom that can be retrieved with the available observed variables. In this section we explore the potential for one additional degree of freedom, by allowing each profile of  $N_w$  to be represented by a linear gradient, as explored in Rose and Chandrasekar (2006) for a dual-frequency retrieval. Here the state vector becomes:

$$\mathbf{x} = \ln \left[ R_1 \cdots R_n \quad \overline{N_w} \quad N_w' \right]^T \quad (12)$$

where  $\overline{N_w}$  is the average  $N_w$  through the profile and  $N_w'$  is the gradient with height.

A retrieval in which  $N_w$  is represented by a linear profile (“linear- $N_w$ ”) is compared against the “constant- $N_w$ ” ZvPIA retrieval, using the average profiles of retrieved and forward-modelled variables for a ZvPIA retrieval of moderate warm rain from Case 3 (Fig. 14). The linear- $N_w$  retrieval significantly improves the fit with 94 GHz observed variables below 1.5 km, where the constant- $N_w$  retrieval underestimates mean Doppler velocity and overestimates radar reflectivity. The linear- $N_w$  retrieval is also better able to forward-model the independent 9.6 GHz radar variables, with near-surface errors in mean Doppler velocity significantly reduced. The linear- $N_w$  retrieval resolves a gradient in  $N_w$  from around  $10^{11} \text{ m}^{-4}$  at cloud-top to  $10^9 \text{ m}^{-4}$

near the surface, and a steeper gradient of  $D_0$ , with corresponding drop size increasing from almost 0.1 mm near cloud-tops to around 0.5 mm at the surface. The changes in  $D_0$  and  $N_w$  through the vertical profile have relatively minor effects on the profile-averaged rain rate, with the retrieved  $R$  increasing somewhat above 2 km, and a decreasing below 0.5 km by around a factor of 2.

- 5 With an additional degree of freedom, the linear- $N_w$  retrieval from 94 GHz radar exhibited increased temporal variability between profiles of the retrieved variables; however, a dual-frequency retrieval (as in Section 5) including a linear representation of  $N_w$  estimated substantially similar profiles of  $N_w$  and  $D_0$  for this case, indicating that the retrieved profiles are robust when better constrained by additional observations. The retrieval of a linear gradient  $N_w$  leads to an improved representation of the vertical profile, both as evaluated against independent 9.6 GHz radar variables, and in that the retrieved profiles of  $N_w$  and  $D_0$
- 10 qualitatively meet expectations for collision and coalescence processes in warm rain. Nevertheless, we note that the profile-averaged  $N_w$  is close to that retrieved with a height-invariant  $N_w$ , and that the corresponding changes in retrieved  $R$  are small in a vertically-averaged sense.

## 7 Discussion and conclusions

The upcoming ESA/JAXA EarthCARE satellite will include ~~the~~ 94 GHz cloud profiling radar, the first Doppler radar in space.

15 In this study we have used ~~airborne Doppler radar~~ ~~aircraft~~ measurements to investigate the prospects for improved ~~global~~ rain retrievals from a spaceborne Doppler radar, with a focus on ~~improving how mean Doppler velocity measurements stand to improve~~ upon 94 GHz radar rain retrievals from CloudSat in two key respects: (1) to facilitate rain rate estimates over land, and; (2) to reduce uncertainties in rain rate estimates by retrieving an additional parameter of the raindrop size distribution (DSD). Retrievals over a range of stratiform rain regimes were made using measurements from the 94 GHz Doppler radar

20 aboard the ER-2 aircraft during the TC4 field campaign over the tropical Pacific in 2007, and evaluated against independent measurements from a less attenuated ~~9.6 GHz Doppler radar~~ ~~second Doppler radar at a less an unattenuated wavelength~~.

The CAPTIVATE algorithm has been developed for rain, cloud and aerosols retrievals from the synergy of active and passive instruments; within the variational scheme, multiple observational variables can be combined as available, and the retrieved variables and their physical representation can be configured at runtime. It is therefore possible with CAPTIVATE

25 to combine the information from multiple radar measurements, and to estimate uncertainties in retrieved variables propagated from uncertainties in the observations and forward-models.

We have shown that the ambiguities of rain rate retrievals ~~at strongly from~~ attenuated radar ~~frequencies~~ can be resolved by either ~~an estimate of path-integrated attenuation (PIA)~~PIA or by the profile of mean Doppler velocity, a measure of drop terminal fallspeed relating to drop size, and which is not affected by partial attenuation of the radar beam. ~~mean Doppler velocity measurements~~.

30 ~~The latter has, with the latter having~~ potential applications to making estimates of rain rate over land, where PIA is more difficult to estimate from the surface backscatter. Furthermore, information from both PIA and mean Doppler velocity can be used to retrieve the rain rate as a function of both median drop size  $D_0$  and drop number concentration  $N_w$ , improving upon significant uncertainties in rain rate estimates owing to assumptions about the DSD.

Retrievals of rain rate  $R$  and drop number concentration  $N_w$  using combined radar reflectivity, PIA and mean Doppler velocity measurements from the 94 GHz radar were evaluated over three cases of tropical stratiform rain over the ocean. The selected cases covered a range of rain rates from virga to heavy showers from rain from both melting ice and liquid clouds. The 94 GHz radar was fully attenuated in profiles with by rain rates around  $10 \text{ mm h}^{-1}$  falling below a melting layer above 4 km, and in rain from slightly heavier rain rates from liquid clouds with tops around 3 km. The attenuation of the 94 GHz radar places an upper limit on the rain profiles that can be retrieved; however, in the mid-latitudes where the melting layer is lower, it may be possible to make retrieval up to higher rain rates before the radar is fully attenuated. The 9.6 GHz radar wavelength was subsequently used included to make a dual-frequency radar retrieval (Section 5). In profiles where the 94 GHz was fully attenuated, the dual-frequency estimates of rain rate were consistent with those derived from the gradient of 94 GHz radar reflectivity. Retrieved values of  $N_w$  ranged from  $10^5 \text{ m}^{-4}$  in light rain from melting ice, with  $D_0$  around 1.0–1.5 mm, up to  $N_w$  of  $10^{10} \text{ m}^{-4}$  in moderate rain from liquid cloud, where  $D_0$  was around 0.1–0.3 mm.

In many contexts collision–coalescence, evaporation and breakup processes are expected to modify the DSD through the vertical profile. With  $N_w$  retrieved as constant with height the retrieval was broadly able to represent the major features of the vertical profile when evaluated against independent 9.6 GHz radar measurements, but errors in the gradient of mean Doppler velocity suggested that the effects of evaporation or collision–coalescence on the DSD through the profile were not resolved. We demonstrated that the 94 GHz radar measurements, including both mean Doppler velocity and PIA, are sufficient to retrieve a more complex representation of  $N_w$  with height (Section 6): in warm rain from liquid cloud it was possible to resolve the decrease in drop concentration and increase in drop size toward the surface consistent with collision–coalescence, while improving on errors with respect to forward-modelled 9.6 GHz radar measurements. The retrieval of a vertical gradient of  $N_w$  has potential applications to both single- and multiple-frequency retrievals of precipitation (e.g. Rose and Chandrasekar, 2006), but must be constrained by sufficient observational variables.

Mean Doppler velocity provides a strong constraint on  $D_0$  that is not compromised by partial attenuation of the radar beam. In combination with radar reflectivity, mean Doppler velocity is sufficient to resolve the ambiguities of radar reflectivity profiles due to attenuation, supporting retrievals of rain rate over land where PIA cannot be estimated from the surface reference technique. In Furthermore, in combination with PIA, the Doppler velocity information provided sufficient information to make robust retrievals of  $R$ - $N_w$  across a range of rain regimes. In light rain with negligible PIA, Doppler velocity is sufficient to retrieve  $R$  and  $N_w$ , suggesting the possibility of using for Doppler radar for  $R$ - $N_w$  retrievals of light rain over land without PIA; however, in moderate rain rates PIA is necessary to constrain the retrieval. Satisfactory retrievals of rain rate may be made over land by assuming  $N_w$  constant, especially for stratiform precipitation, or PIA could be estimated from the land surface backscatter with a large observational uncertainty (as in Iguchi et al., 2009), which may provide sufficient information to resolve the ambiguity between weakly and strongly attenuating profiles. A robust method of using Doppler radar to estimating rain rate over land will be the subject of future work.

With a constraint on PIA, the gradient of apparent radar reflectivity can be used to estimate  $R$ . While Doppler velocity is generally required to retrieve  $N_w$ , in moderate warm rain from liquid clouds the combination of low radar reflectivity and strong attenuation was sufficient to retrieve the high concentration of small drops typical of warm rain, without the need for Doppler

velocity information: this finding may be applicable to retrievals of the drop number concentration in warm rain observed by CloudSat.

We have demonstrated the contribution of mean Doppler velocity to assimilating drop size information in estimates of rain rate. With the first Doppler radar in space, EarthCARE synergy retrievals will exploit novel measurements to improve the EarthCARE will make a significant contribution to the satellite remote sensing of clouds and precipitation rain. Mean Doppler velocity provides an effective constraint on drop size that can be exploited to estimate rain rate over land, and to reduce uncertainty in rain rate estimates through the vertical profile by retrieving the drop number concentration  $N_w$  of the rain DSD, which must otherwise be assumed. Future work will focus on understanding the application of these retrievals to spaceborne Doppler radar, including the effects of multiple scattering and non-uniform beam filling on the Doppler measurements. As part of EarthCARE radar–lidar–radiometer synergy retrievals, improved global estimates of rain rate and drop size from Doppler radar will provide new insights into the interactions of clouds, aerosols and precipitation through the atmospheric profile.

*Acknowledgements.* This work was supported by the National Centre for Earth Observation (NCEO) and European Space Agency Grant 4000112030/15/NL/CT, with computing resources provided by the University of Reading. Dr. Tian’s research is supported by NASA Precipitation Measurement Mission and Remote Sensing Theory. We thank Gerry Heymsfield and the ER-2 radar engineers for collecting CRS and EDOP data, Dennis Hlavka (NASA-GSFC) for assistance with CPL data, and Stephen Platnick and Howard Tan (NASA-JPL) with MAS/MASTER radiometer data. ERA-Interim data are produced and distributed by ECMWF, and hosted by the Centre for Environmental Data Analysis.

We are grateful to Alain Protat and two anonymous referees for their constructive feedback, and Ross Bannister, Nancy Nichols, Lars Isaksen, Elias Holm and Mike Rennie for helpful discussions.

## References

- Abel, S. J. and Boutle, I. A.: An improved representation of the raindrop size distribution for single-moment microphysics schemes, *Quarterly Journal of the Royal Meteorological Society*, 138, 2151–2162, doi:10.1002/qj.1949, 2012.
- Atlas, D., Srivastava, R., and Sekhon, R.: Doppler radar characteristics of precipitation at vertical incidence, *Reviews of Geophysics*, 1973.
- 5 Battaglia, A. and Tanelli, S.: DOMUS: DOppler MUltiple-Scattering Simulator, *IEEE Transactions on Geoscience and Remote Sensing*, 49, 442–450, doi:10.1109/TGRS.2010.2052818, 2011.
- Battaglia, A., Ajewole, M. O., and Simmer, C.: Multiple scattering effects due to hydrometeors on precipitation radar systems, *Geophysical Research Letters*, 32, n/a–n/a, doi:10.1029/2005GL023810, 2005.
- Battaglia, A., Ajewole, M. O., and Simmer, C.: Evaluation of radar multiple scattering effects in Cloudsat configuration, *Atmospheric*  
10 *Chemistry and Physics*, 7, 1719–1730, doi:10.5194/acp-7-1719-2007, 2007.
- Beard, K. V.: Terminal Velocity and Shape of Cloud and Precipitation Drops Aloft, *Journal of the Atmospheric Sciences*, 33, 851–864, doi:10.1175/1520-0469(1976)033<0851:TVASOC>2.0.CO;2, 1976.
- Behrangi, A., Lebsock, M., Wong, S., and Lambriksen, B.: On the quantification of oceanic rainfall using spaceborne sensors, *Journal of Geophysical Research: Atmospheres*, 117, doi:10.1029/2012JD017979, 2012.
- 15 Berg, W., L'Ecuyer, T., Haynes, J. M., Berg, W., L'Ecuyer, T., and Haynes, J. M.: The Distribution of Rainfall over Oceans from Spaceborne Radars, *Journal of Applied Meteorology and Climatology*, 49, 535–543, doi:10.1175/2009JAMC2330.1, 2010.
- Ceccaldi, M., Delanoë, J., Hogan, R. J., Pounder, N. L., Protat, A., and Pelon, J.: From CloudSat-CALIPSO to EarthCare: Evolution of the DARDAR cloud classification and its comparison to airborne radar-lidar observations, *Journal of Geophysical Research: Atmospheres*, 118, 7962–7981, doi:10.1002/jgrd.50579, 2013.
- 20 Dee, D. P., Uppala, S. M., Simmons, A. J., Berrisford, P., Poli, P., Kobayashi, S., Andrae, U., Balmaseda, M. A., Balsamo, G., Bauer, P., Bechtold, P., Beljaars, A. C. M., van de Berg, L., Bidlot, J., Bormann, N., Delsol, C., Dragani, R., Fuentes, M., Geer, A. J., Haimberger, L., Healy, S. B., Hersbach, H., H<sub>v</sub>lm, E. V., Isaksen, I., K<sub>v</sub>llberg, P., K<sub>v</sub>hler, M., Matricardi, M., McNally, A. P., Monge-Sanz, B. M., Morcrette, J. J., Park, B. K., Peubey, C., de Rosnay, P., Tavolato, C., Th<sub>e</sub>paut, J. N., and Vitart, F.: The ERA-Interim reanalysis: configuration and performance of the data assimilation system, *Quarterly Journal of the Royal Meteorological Society*, 137, 553–597,  
25 doi:10.1002/qj.828, 2011.
- Firda, J. M., Sekelsky, S. M., McIntosh, R. E., Firda, J. M., Sekelsky, S. M., and McIntosh, R. E.: Application of Dual-Frequency Millimeter-Wave Doppler Spectra for the Retrieval of Drop Size Distributions and Vertical Air Motion in Rain, *Journal of Atmospheric and Oceanic Technology*, 16, 216–236, doi:10.1175/1520-0426(1999)016<0216:AODFMW>2.0.CO;2, 1999.
- Frisch, A. S., Fairall, C. W., and Snider, J. B.: Measurement of Stratus Cloud and Drizzle Parameters in ASTEX with a K<sub>α</sub>-  
30 -Band Doppler Radar and a Microwave Radiometer, *Journal of the Atmospheric Sciences*, 52, 2788–2799, doi:10.1175/1520-0469(1995)052<2788:MOSCAD>2.0.CO;2, 1995.
- Hawkness-Smith, L.: A novel retrieval of liquid water path and a evaluation of the representation of drizzle in numerical models, Ph.D. thesis, University of Reading, <http://ethos.bl.uk/OrderDetails.do?uin=uk.bl.ethos.533772>, 2010.
- Haynes, J. M., L'Ecuyer, T. S., Stephens, G. L., Miller, S. D., Mitrescu, C., Wood, N. B., and Tanelli, S.: Rainfall retrieval over the ocean with spaceborne W-band radar, *Journal of Geophysical Research*, 114, D00A22, doi:10.1029/2008JD009973, 2009.
- Haynes, J. M., Jakob, C., Rossow, W. B., Tselioudis, G., and Brown, J. R.: Major Characteristics of Southern Ocean Cloud Regimes and Their Effects on the Energy Budget, *Journal of Climate*, 24, 5061–5080, doi:10.1175/2011JCLI4052.1, 2011.

- Heymsfield, G. M., Bidwell, S. W., Caylor, I. J., Ameen, S., Nicholson, S., Boncyk, W., Miller, L., Vandemark, D., Racette, P. E., and Dod, L. R.: The EDOP Radar System on the High-Altitude NASA ER-2 Aircraft, *Journal of Atmospheric and Oceanic Technology*, 13, 795–809, doi:10.1175/1520-0426(1996)013<0795:TERSOT>2.0.CO;2, 1996.
- Hitschfeld, W. and Bordan, J.: ERRORS INHERENT IN THE RADAR MEASUREMENT OF RAINFALL AT ATTENUATING WAVE-  
5 LENGTHS, *Journal of Meteorology*, 11, 58–67, doi:10.1175/1520-0469(1954)011<0058:EIITRM>2.0.CO;2, 1954.
- Hogan, R. J.: A Variational Scheme for Retrieving Rainfall Rate and Hail Reflectivity Fraction from Polarization Radar, *Journal of Applied Meteorology and Climatology*, 46, 1544–1564, doi:10.1175/JAM2550.1, 2007.
- Hogan, R. J.: Fast Lidar and Radar Multiple-Scattering Models. Part I: Small-Angle Scattering Using the Photon Variance–Covariance Method, *Journal of the Atmospheric Sciences*, 65, 3621–3635, doi:10.1175/2008JAS2642.1, 2008.
- 10 Hook, S. J. S., Myers, J. J. J., Thome, K. K. J., Fitzgerald, M., and Kahle, A. B.: The MODIS/ASTER airborne simulator (MASTER) — a new instrument for earth science studies, *Remote Sensing of Environment*, 76, 93–102, doi:10.1016/S0034-4257(00)00195-4, 2001.
- Hou, A. Y., Kakar, R. K., Neeck, S., Azarbarzin, A. A., Kummerow, C. D., Kojima, M., Oki, R., Nakamura, K., Iguchi, T., Hou, A. Y., Kakar, R. K., Neeck, S., Azarbarzin, A. A., Kummerow, C. D., Kojima, M., Oki, R., Nakamura, K., and Iguchi, T.: The Global Precipitation Measurement Mission, *Bulletin of the American Meteorological Society*, 95, 701–722, doi:10.1175/BAMS-D-13-00164.1, 2014.
- 15 Iguchi, T., Kozu, T., Meneghini, R., Awaka, J., Okamoto, K., Iguchi, T., Kozu, T., Meneghini, R., Awaka, J., and Okamoto, K.: Rain-Profiling Algorithm for the TRMM Precipitation Radar, *Journal of Applied Meteorology*, 39, 2038–2052, doi:10.1175/1520-0450(2001)040<2038:RPAFTT>2.0.CO;2, 2000.
- Iguchi, T., Kozu, T., Kwaitkowski, J., Meneghini, R., Awaka, J., and Okamoto, K.: Uncertainties in the Rain Profiling Algorithm for the TRMM Precipitation Radar, *Journal of the Meteorological Society of Japan*, 87A, 1–30, doi:10.2151/jmsj.87A.1, 2009.
- 20 Illingworth, A. J. and Blackman, T. M.: The Need to Represent Raindrop Size Spectra as Normalized Gamma Distributions for the Interpretation of Polarization Radar Observations, *Journal of Applied Meteorology*, 41, 286–297, doi:10.1175/1520-0450(2002)041<0286:TNTRRS>2.0.CO;2, 2002.
- Illingworth, A. J., Barker, H. W., Beljaars, A., Ceccaldi, M., Chepfer, H., Clerbaux, N., Cole, J., Delanoë, J., Domenech, C., Donovan, D. P., Fukuda, S., Hiraakata, M., Hogan, R. J., Huenerbein, A., Kollias, P., Kubota, T., Nakajima, T., Nakajima, T. Y., Nishizawa, T., Ohno, Y.,  
25 Okamoto, H., Oki, R., Sato, K., Satoh, M., Shephard, M. W., Velázquez-Blázquez, A., Wandinger, U., Wehr, T., and van Zadelhoff, G.-J.: The EarthCARE Satellite: The Next Step Forward in Global Measurements of Clouds, Aerosols, Precipitation, and Radiation, *Bulletin of the American Meteorological Society*, 96, 1311–1332, doi:10.1175/BAMS-D-12-00227.1, 2015.
- King, M. D., Menzel, W. P., Grant, P. S., Myers, J. S., Arnold, G. T., Platnick, S. E., Gumley, L. E., Tsay, S.-C., Moeller, C. C., Fitzgerald, M., Brown, K. S., Osterwisch, F. G., King, M. D., Menzel, W. P., Grant, P. S., Myers, J. S., Arnold, G. T., Platnick, S. E., Gumley, L. E.,  
30 Tsay, S.-C., Moeller, C. C., Fitzgerald, M., Brown, K. S., and Osterwisch, F. G.: Airborne Scanning Spectrometer for Remote Sensing of Cloud, Aerosol, Water Vapor, and Surface Properties, *Journal of Atmospheric and Oceanic Technology*, 13, 777–794, doi:10.1175/1520-0426(1996)013<0777:ASSFRS>2.0.CO;2, 1996.
- Kollias, P., Rémillard, J., Luke, E., and Szyrmer, W.: Cloud radar Doppler spectra in drizzling stratiform clouds: 1. Forward modeling and remote sensing applications, *Journal of Geophysical Research*, 116, D13 201, doi:10.1029/2010JD015237, 2011a.
- 35 Kollias, P., Szyrmer, W., Rémillard, J., and Luke, E.: Cloud radar Doppler spectra in drizzling stratiform clouds: 2. Observations and micro-physical modeling of drizzle evolution, *Journal of Geophysical Research*, 116, D13 203, doi:10.1029/2010JD015238, 2011b.

- Kummerow, C., Barnes, W., Kozu, T., Shiue, J., Simpson, J., Kummerow, C., Barnes, W., Kozu, T., Shiue, J., and Simpson, J.: The Tropical Rainfall Measuring Mission (TRMM) Sensor Package, *Journal of Atmospheric and Oceanic Technology*, 15, 809–817, doi:10.1175/1520-0426(1998)015<0809:TTRMMT>2.0.CO;2, 1998.
- Lebsock, M., Morrison, H., and Gettelman, A.: Microphysical implications of cloud-precipitation covariance derived from satellite remote sensing, *Journal of Geophysical Research: Atmospheres*, 118, 6521–6533, doi:10.1002/jgrd.50347, 2013.
- Lebsock, M. D. and L'Ecuyer, T. S.: The retrieval of warm rain from CloudSat, *Journal of Geophysical Research: Atmospheres*, 116, D20 209, doi:10.1029/2011JD016076, 2011.
- Lebsock, M. D., L'Ecuyer, T. S., and Stephens, G. L.: Detecting the Ratio of Rain and Cloud Water in Low-Latitude Shallow Marine Clouds, *Journal of Applied Meteorology and Climatology*, 50, 419–432, doi:10.1175/2010JAMC2494.1, 2011.
- 10 L'Ecuyer, T. S. and Stephens, G. L.: An Estimation-Based Precipitation Retrieval Algorithm for Attenuating Radars, *Journal of Applied Meteorology*, 41, 272–285, doi:10.1175/1520-0450(2002)041<0272:AEBPRA>2.0.CO;2, 2002.
- Li, L., Heymsfield, G. M., Racette, P. E., Tian, L., and Zenker, E.: A 94-GHz Cloud Radar System on a NASA High-Altitude ER-2 Aircraft, *Journal of Atmospheric and Oceanic Technology*, 21, 1378–1388, doi:10.1175/1520-0426(2004)021<1378:AGCRSO>2.0.CO;2, 2004.
- Liao, L., Meneghini, R., Tian, L., and Heymsfield, G. M.: Retrieval of Snow and Rain From Combined X- and W-Band Airborne Radar Measurements, *IEEE Transactions on Geoscience and Remote Sensing*, 46, 1514–1524, doi:10.1109/TGRS.2008.916079, 2008.
- 15 Liao, L., Meneghini, R., Tian, L., and Heymsfield, G. M.: Measurements and Simulations of Nadir-Viewing Radar Returns from the Melting Layer at X and W Bands, *Journal of Applied Meteorology and Climatology*, 48, 2215–2226, doi:10.1175/2009JAMC2033.1, 2009.
- Liebe, H. J.: An updated model for millimeter wave propagation in moist air, *Radio Science*, 20, 1069–1089, 1985.
- Luke, E. P. and Kollias, P.: Separating Cloud and Drizzle Radar Moments during Precipitation Onset Using Doppler Spectra, *Journal of Atmospheric and Oceanic Technology*, 30, 1656–1671, doi:10.1175/JTECH-D-11-00195.1, 2013.
- 20 Mace, G. G., Avey, S., Cooper, S., Lebsock, M., Tanelli, S., and Dobrowalski, G.: Retrieving co-occurring cloud and precipitation properties of warm marine boundary layer clouds with A-Train data, *Journal of Geophysical Research: Atmospheres*, 121, 4008–4033, doi:10.1002/2015JD023681, 2016.
- Marshall, J. and Palmer, W.: The distribution of raindrops with size, *Journal of meteorology*, 1948.
- 25 Matrosov, S.: Assessment of Radar Signal Attenuation Caused by the Melting Hydrometeor Layer, *IEEE Transactions on Geoscience and Remote Sensing*, 46, 1039–1047, doi:10.1109/TGRS.2008.915757, 2008.
- Matrosov, S. Y.: Potential for attenuation-based estimations of rainfall rate from CloudSat, *Geophysical Research Letters*, 34, L05 817, doi:10.1029/2006GL029161, 2007.
- McGill, M., Hlavka, D., Hart, W., Scott, V. S., Spinhirne, J., and Schmid, B.: Cloud Physics Lidar: instrument description and initial measurement results, *Applied Optics*, 41, 3725, doi:10.1364/AO.41.003725, 2002.
- 30 McGill, M. J.: Combined lidar-radar remote sensing: Initial results from CRYSTAL-FACE, *Journal of Geophysical Research*, 109, D07 203, doi:10.1029/2003JD004030, 2004.
- Meneghini, R. and Liao, L.: Effective Dielectric Constants of Mixed-Phase Hydrometeors, *Journal of Atmospheric and Oceanic Technology*, 17, 628–640, doi:10.1175/1520-0426(2000)017<0628:EDCOMP>2.0.CO;2, 2000.
- 35 Meneghini, R., Eckerman, J., and Atlas, D.: Determination of Rain Rate from a Spaceborne Radar Using Measurements of Total Attenuation, *IEEE Transactions on Geoscience and Remote Sensing*, GE-21, 34–43, doi:10.1109/TGRS.1983.350528, 1983.
- Mie, G.: Beiträge zur Optik trüber Medien, speziell kolloidaler Metallösungen, *Annalen der Physik*, 330, 377–445, doi:10.1002/andp.19083300302, 1908.

- Mishchenko, M. I., Travis, L. D., and Mackowski, D. W.: T-matrix computations of light scattering by nonspherical particles: A review, *Journal of Quantitative Spectroscopy and Radiative Transfer*, 55, 535–575, doi:10.1016/0022-4073(96)00002-7, 1996.
- Moisseev, D. N. and Chandrasekar, V.: Examination of the  $\mu$ - $\lambda$  Relation Suggested for Drop Size Distribution Parameters, *Journal of Atmospheric and Oceanic Technology*, 24, 847–855, doi:10.1175/JTECH2010.1, 2007.
- 5 Nelson, E. L., L'Ecuyer, T. S., Saleeby, S. M., Berg, W., Herbener, S. R., van den Heever, S. C., Nelson, E. L., L'Ecuyer, T. S., Saleeby, S. M., Berg, W., Herbener, S. R., and Heever, S. C. v. d.: Toward an Algorithm for Estimating Latent Heat Release in Warm Rain Systems, *Journal of Atmospheric and Oceanic Technology*, 33, 15–0205, doi:10.1175/JTECH-D-15-0205.1, 2016.
- O'Connor, E. J., Hogan, R. J., and Illingworth, A. J.: Retrieving Stratocumulus Drizzle Parameters Using Doppler Radar and Lidar, *Journal of Applied Meteorology*, 44, 14–27, doi:10.1175/JAM-2181.1, 2005.
- 10 Rapp, A. D., Lebsock, M., L'Ecuyer, T., and L'Ecuyer, T.: Low cloud precipitation climatology in the southeastern Pacific marine stratocumulus region using CloudSat, *Environmental Research Letters*, 8, 014 027, doi:10.1088/1748-9326/8/1/014027, 2013.
- Rodgers, C.: *Inverse methods for atmospheric sounding: theory and practice*, World Scientific, 2000.
- Rose, C. R. and Chandrasekar, V.: A GPM Dual-Frequency Retrieval Algorithm: DSD Profile-Optimization Method, *Journal of Atmospheric and Oceanic Technology*, 23, 1372–1383, doi:10.1175/JTECH1921.1, 2006.
- 15 Stephens, G. L., Vane, D. G., Boain, R. J., Mace, G. G., Sassen, K., Wang, Z., Illingworth, A. J., O'Connor, E. J., Rossow, W. B., Durden, S. L., and others: The CloudSat mission and the A-Train, *Bulletin of the American Meteorological Society*, 83, 1771–1790, 2002.
- Stephens, G. L., L'Ecuyer, T., Forbes, R., Gettleman, A., Golaz, J.-C., Bodas-Salcedo, A., Suzuki, K., Gabriel, P., and Haynes, J.: Dreary state of precipitation in global models, *Journal of Geophysical Research*, 115, D24 211, doi:10.1029/2010JD014532, 2010.
- Testud, J., Oury, S., Black, R. A., Amayenc, P., and Dou, X.: The Concept of “Normalized” Distribution to Describe Raindrop Spectra: A Tool for Cloud Physics and Cloud Remote Sensing, *Journal of Applied Meteorology*, 40, 1118–1140, doi:10.1175/1520-0450(2001)040<1118:TCOND>2.0.CO;2, 2001.
- 20 Thurai, M., Huang, G. J., Bringi, V. N., Randeu, W. L., Schönhuber, M., Thurai, M., Huang, G. J., Bringi, V. N., Randeu, W. L., and Schönhuber, M.: Drop Shapes, Model Comparisons, and Calculations of Polarimetric Radar Parameters in Rain, *Journal of Atmospheric and Oceanic Technology*, 24, 1019–1032, doi:10.1175/JTECH2051.1, 2007.
- 25 Tian, L., Heymsfield, G. M., Li, L., and Srivastava, R. C.: Properties of light stratiform rain derived from 10- and 94-GHz airborne Doppler radars measurements, *Journal of Geophysical Research*, 112, D11 211, doi:10.1029/2006JD008144, 2007.
- Tokay, A. and Short, D. A.: Evidence from Tropical Raindrop Spectra of the Origin of Rain from Stratiform versus Convective Clouds, *Journal of Applied Meteorology*, 35, 355–371, doi:10.1175/1520-0450(1996)035<0355:EFTRSO>2.0.CO;2, 1996.
- Toon, O. B. O., Starr, D. O. D., Jensen, E. J., Newman, P. A., Platnick, S., Schoeberl, M. R., Wennberg, P. O., Wofsy, S. C., Kurylo, M. J., Maring, H., Jucks, K. W., Craig, M. S., Vasques, M. F., Pfister, L., Rosenlof, K. H., Selkirk, H. B., Colarco, P. R., Kawa, S. R., Mace, G. G., Minnis, P., and Pickering, K. E.: Planning, implementation, and first results of the Tropical Composition, Cloud and Climate Coupling Experiment (TC4), *Journal of Geophysical Research*, 115, D00J04, doi:10.1029/2009JD013073, 2010.
- 30 Twomey, S.: *Introduction to the Mathematics of Inversion in Remote Sensing and Indirect, Measurement* Elsevier Scientific Publishing Co, 1977.
- 35 Weston, P. P., Bell, W., and Eyre, J. R.: Accounting for correlated error in the assimilation of high-resolution sounder data, *Quarterly Journal of the Royal Meteorological Society*, 140, 2420–2429, doi:10.1002/qj.2306, 2014.

- Wilson, D. R., Illingworth, A. J., Blackman, T. M., Wilson, D. R., Illingworth, A. J., and Blackman, T. M.: Differential Doppler Velocity: A Radar Parameter for Characterizing Hydrometeor Size Distributions, *Journal of Applied Meteorology*, 36, 649–663, doi:10.1175/1520-0450-36.6.649, 1997.
- 5 Wood, R., Kubar, T. L., Hartmann, D. L., and Wood, R.: Understanding the Importance of Microphysics and Macrophysics for Warm Rain in Marine Low Clouds. Part II: Heuristic Models of Rain Formation, *Journal of the Atmospheric Sciences*, 66, 2953–2972, doi:10.1175/2009JAS3072.1, 2009.
- Yoshida, R., Okamoto, H., Hagihara, Y., and Ishimoto, H.: Global analysis of cloud phase and ice crystal orientation from Cloud-Aerosol Lidar and Infrared Pathfinder Satellite Observation (CALIPSO) data using attenuated backscattering and depolarization ratio, *Journal of Geophysical Research*, 115, D00H32, doi:10.1029/2009JD012334, 2010.
- 10 Zhang, G., Vivekanandan, J., and Brandes, E.: A method for estimating rain rate and drop size distribution from polarimetric radar measurements, *IEEE Transactions on Geoscience and Remote Sensing*, 39, 830–841, doi:10.1109/36.917906, 2001.

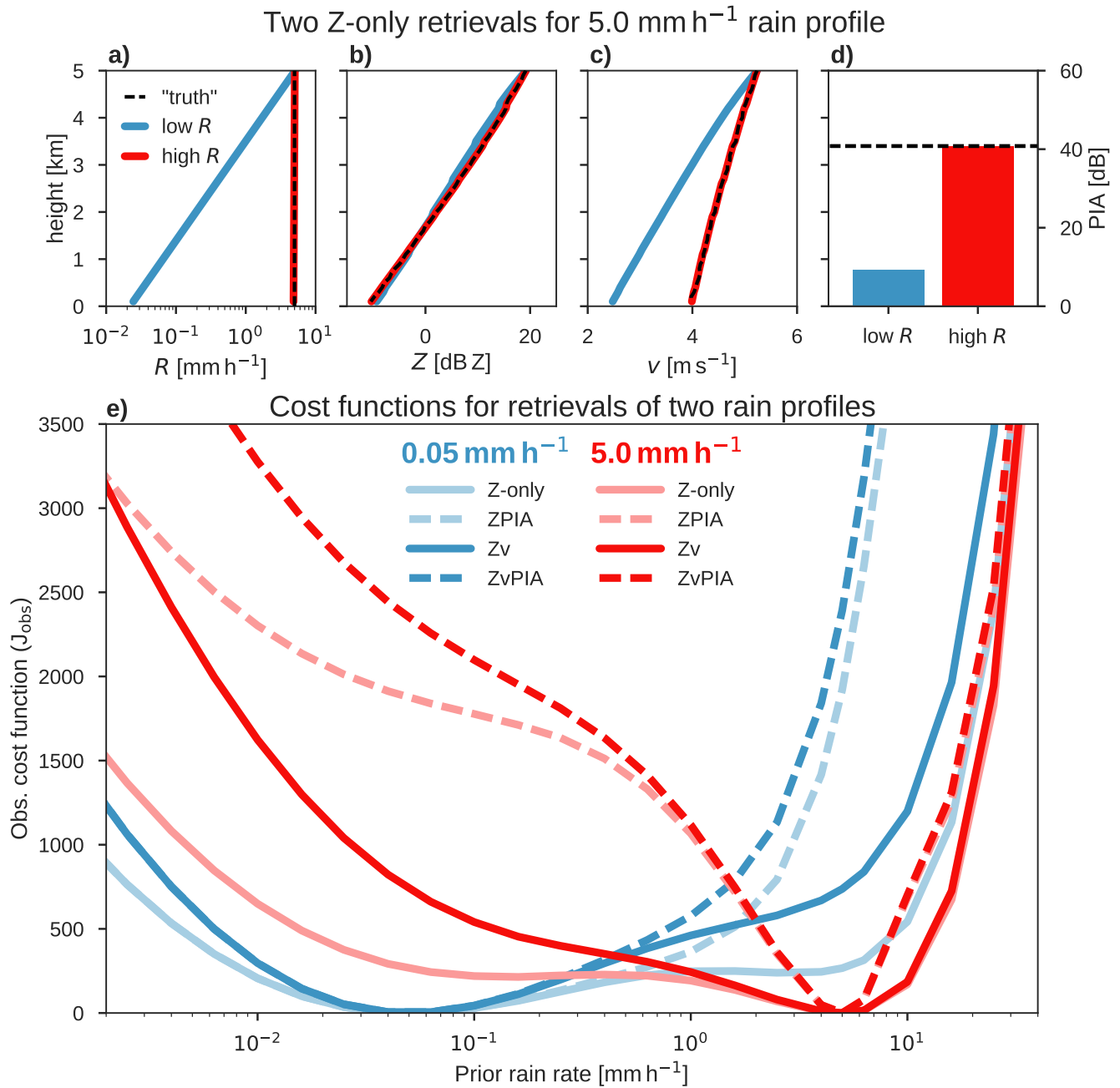


**Figure 1.** Above: Profiles of (a) retrieved rain rate, and (b) forward-modelled 94GHz radar reflectivity, (c) mean Doppler velocity and (d) PIA, for the two solutions to the retrieval from a synthetic profile; dashed lines show the values corresponding to the “true” profile of constant  $R = 5.0 \text{ mm h}^{-1}$ .

Below: (e) the observational component of the cost function ( $J_{\text{obs}}$ ) for retrievals of two constant rain profiles with  $R = 0.05 \text{ mm h}^{-1}$  and  $R = 5.0 \text{ mm h}^{-1}$ , initialised from a range of  $R$  priors. Bimodal or ambiguous retrievals are evident when using radar reflectivity alone (Z-only; light solid lines), and compared against retrievals using additional observational variables (Zv, ZPIA, and ZvPIA; dashed and dark lines) to resolve the ambiguity.

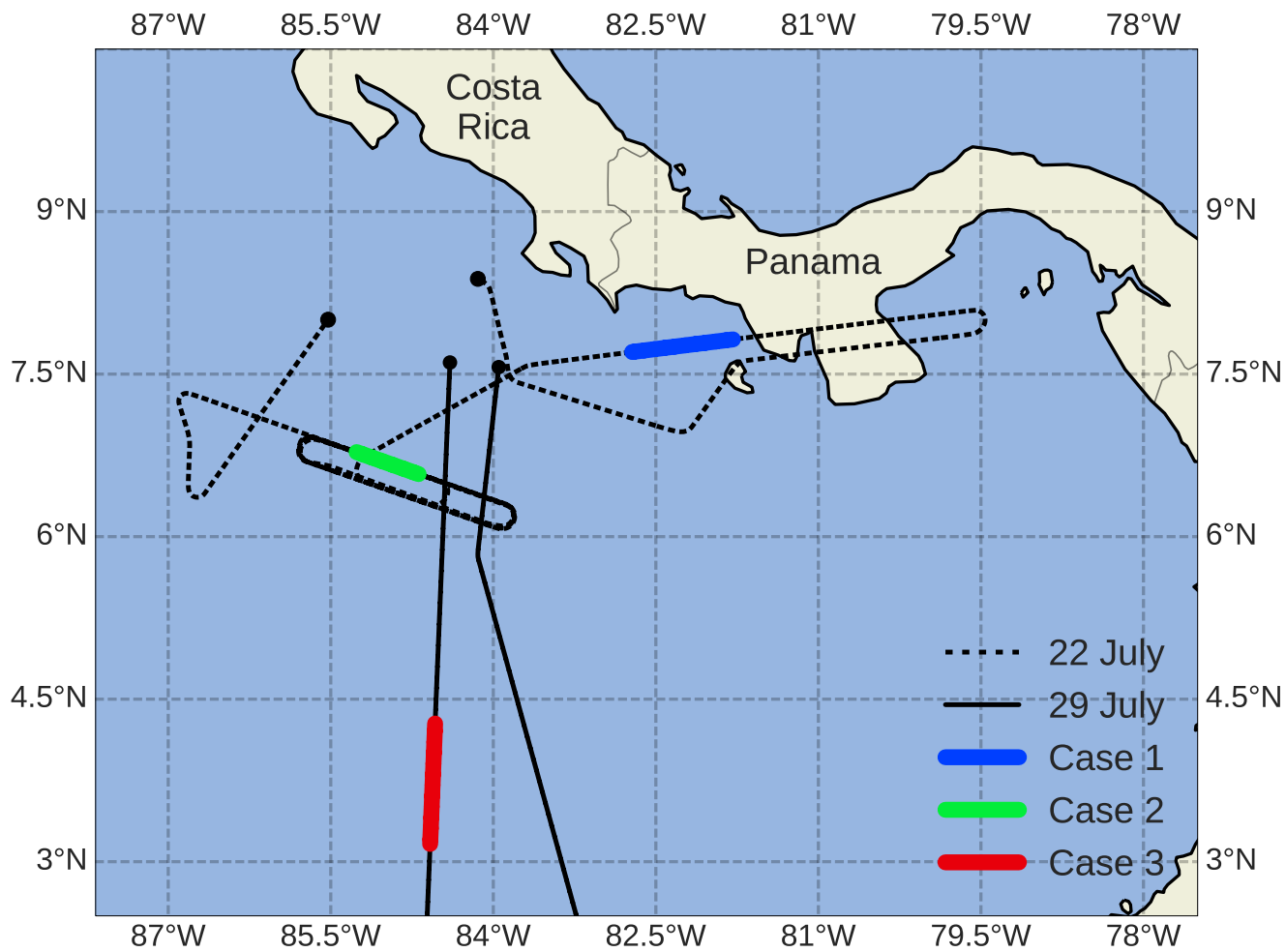


**Figure 2.** Flight tracks of the NASA ER-2 high-altitude aircraft over the tropical eastern Pacific on 22 July and 29 July 2007 during the TC4 field campaign. The flight legs selected for case studies of stratiform rain are highlighted.

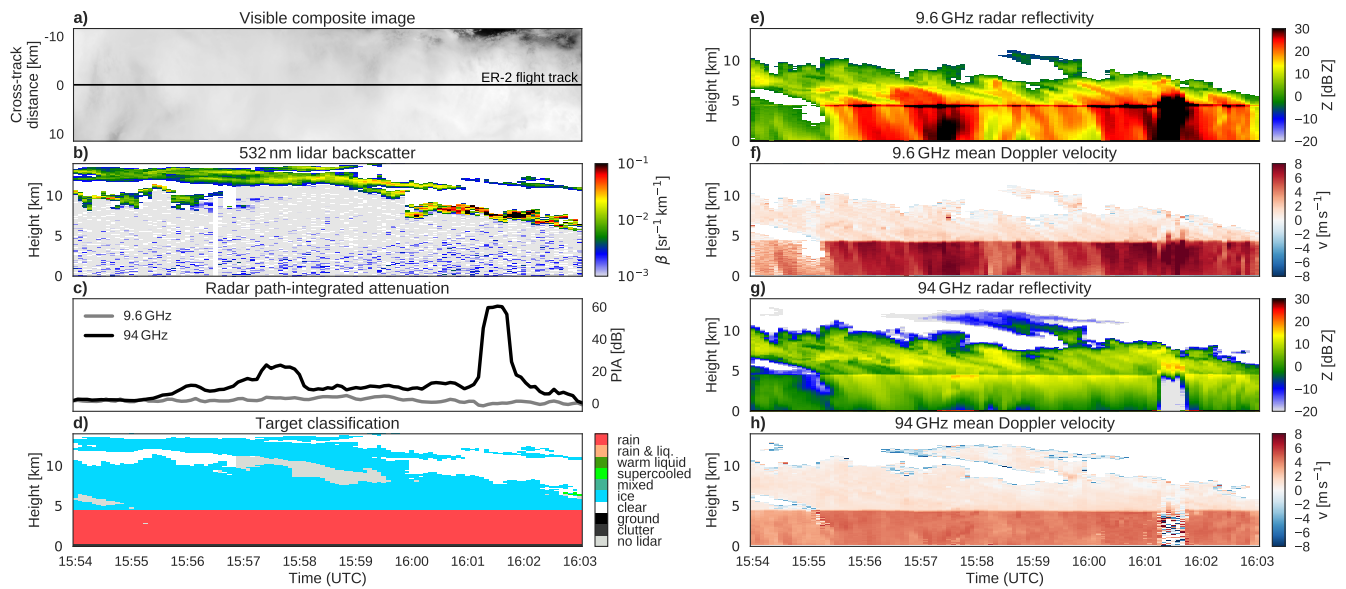


**Figure 3.** Selected measurements made by ER-2 instruments for Case 1 between 15:53 and 16:03 UTC on 22 July 2007 as part of TC4. Composite cloud scene (a) from MAS/MASTER visible channels, with the ER-2 flight track marked; 532nm lidar backscatter (b); 9.6 and 94 GHz radar PIA (c); target classification from radar-lidar synergy (d); 9.6 GHz radar reflectivity (e) and mean Doppler velocity (f); and 94 GHz radar reflectivity (g) and mean Doppler velocity (h).

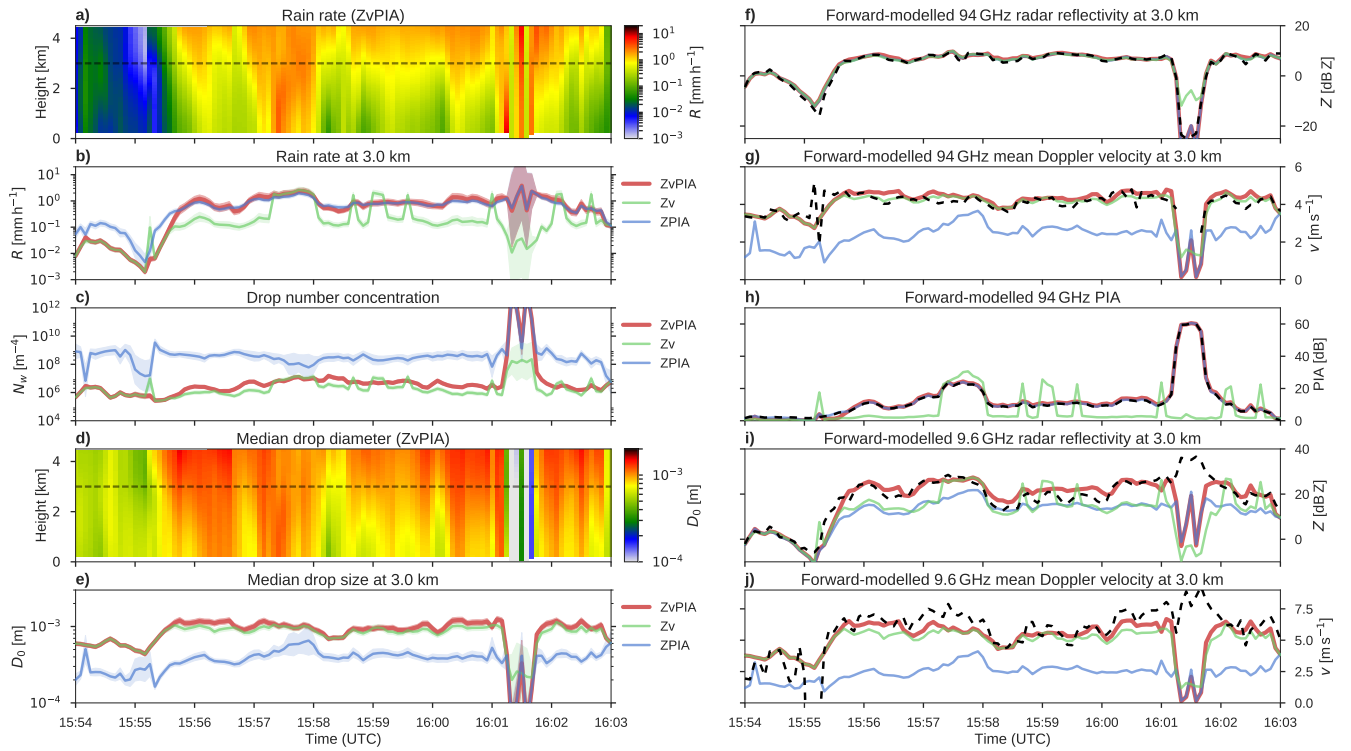


**Figure 4.** Time series of 94 GHz ZPIA,  $Z_v$  and  $Z_v\text{PIA}$  retrievals compared for Case 1 between 15:54 and 16:13 on 22 July 2007. Retrieved state and derived variables (left), and forward-modelled radar measurements (right) for the three retrievals are shown at a height of 3 km above sea level (indicated with a light dashed line in the left-hand scenes), while the full scenes of  $R$  (a) and  $D_0$  (d) are shown for the  $Z_v\text{PIA}$  retrieval. Shading indicates the  $1-\sigma$  uncertainty in the retrieved and derived variables. Dark dashed lines (right) indicate the observed radar measurements.

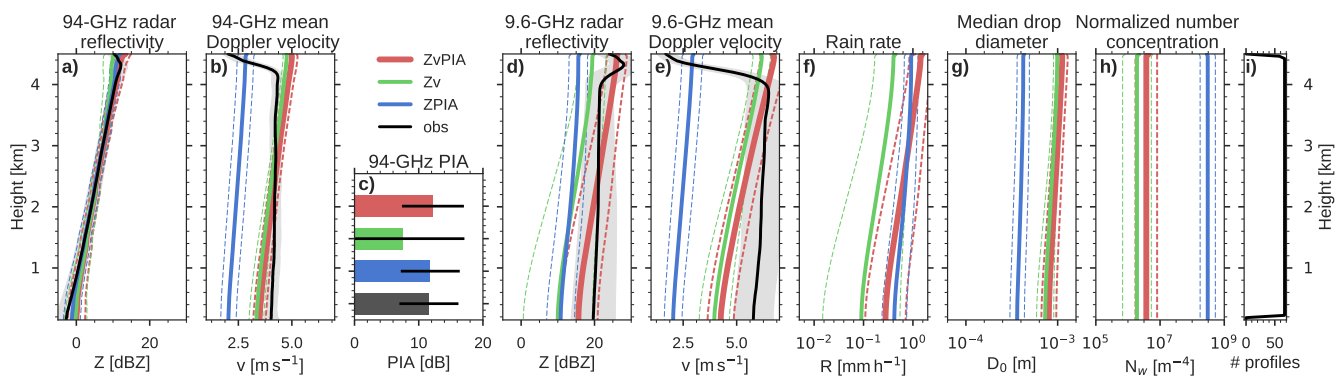


**Figure 5.** Averaged profiles of moderate rain between 15:55:30 and 16:11:00 UTC on 22 July 2007. Forward-modelled 94 GHz radar reflectivity (a), mean Doppler velocity (b) and PIA (c); forward-modelled 9.6 GHz radar reflectivity (d) and mean Doppler velocity (e); and retrieved rain rate (f), median drop size (g), number concentration parameter (h) for ZPIA, Zv and ZvPIA retrievals. The number of profiles included at each height is indicated in (i). Shading and dashed lines indicate the  $1\text{-}\sigma$  uncertainty in the retrieved and derived variables.

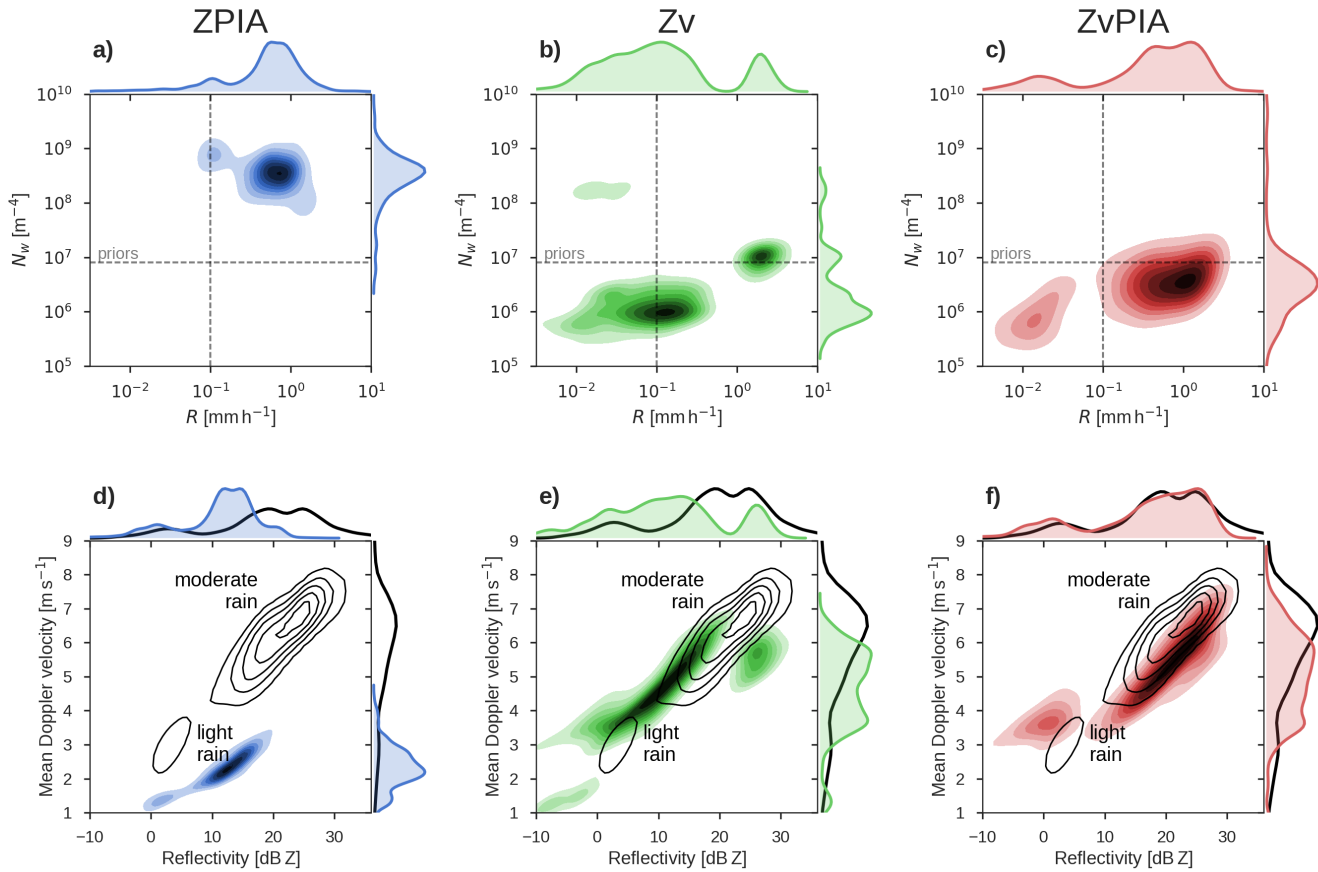


**Figure 6.** Joint (filled contours) and univariate (curves) kernel density estimation histograms of retrieved rain state variables  $R$  and  $N_w$  (a–c) and forward-modelled EDOP measurements (d–f) for ZPIA (a and d), Zv (b and e) and ZvPIA (c and f) rain retrievals during Case 1 on 22 July 2007. Dashed lines indicate the values of the prior state variables used in the retrieval. Black contours indicate the distribution of independent EDOP measurements; the major rain regimes are labelled.

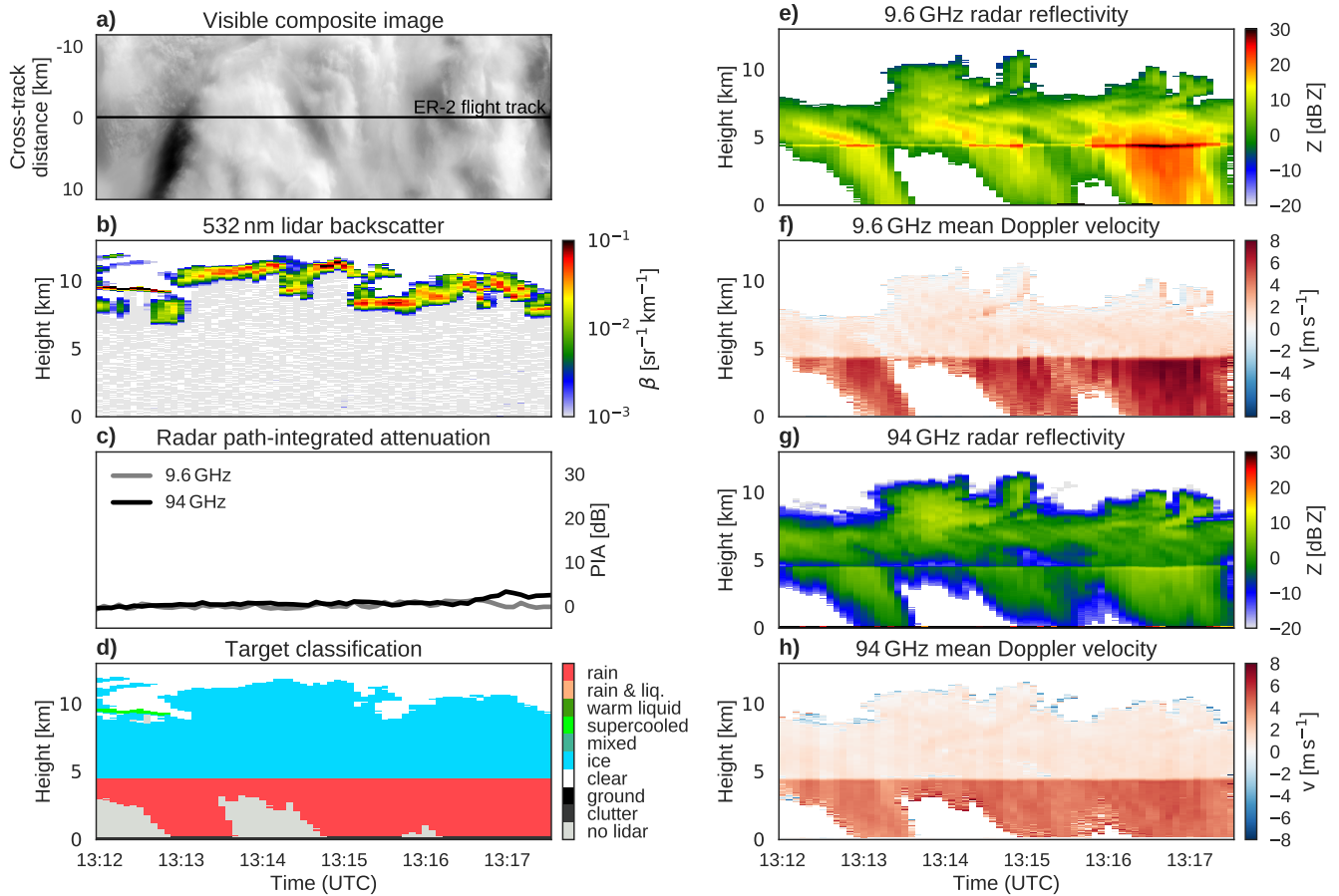


**Figure 7.** Selected measurements made by ER-2 instruments for Case 2 between 13:12:00 and 13:17:30 UTC on 22 July 2007 as part of TC4. The composite cloud image from MAS/MASTER visible channels (a), with the ER-2 flight track marked; 532 nm lidar backscatter (b); 9.6 and 94 GHz radar PIA (c); target classification from radar–lidar synergy (d); 9.6 GHz radar reflectivity (e) and mean Doppler velocity (f); and 94 GHz radar reflectivity (g) and mean Doppler velocity (h).

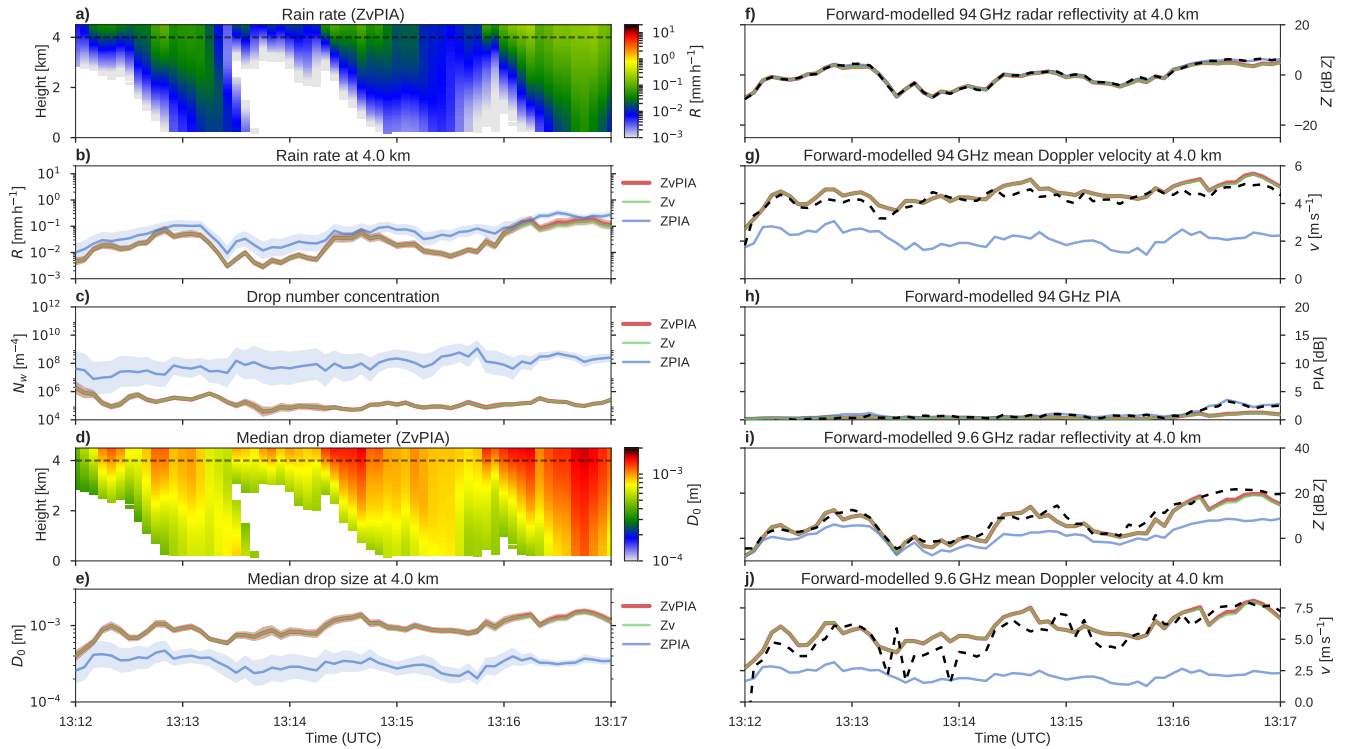


**Figure 8.** Time series of 94 GHz ZPIA, Zv and ZvPIA retrievals compared for Case 2 between 13:12 and 13:17 on 22 July 2007. Retrieved state and derived variables (left), and forward-modelled radar measurements (right) for the three retrievals are shown at a height of 4 km above sea level (indicated with a dashed line in the left-hand scenes), while the full scenes of  $R$  (a) and  $D_0$  (d) are shown for the ZvPIA retrieval. In this case the observed PIA is negligible, so the ZvPIA retrieval has no more information than the Zv retrieval and the two lines are overlaid. Shading indicates the 1- $\sigma$  uncertainty in the retrieved and derived variables. Black dashed lines indicate the observed radar measurements for comparison with the retrievals.

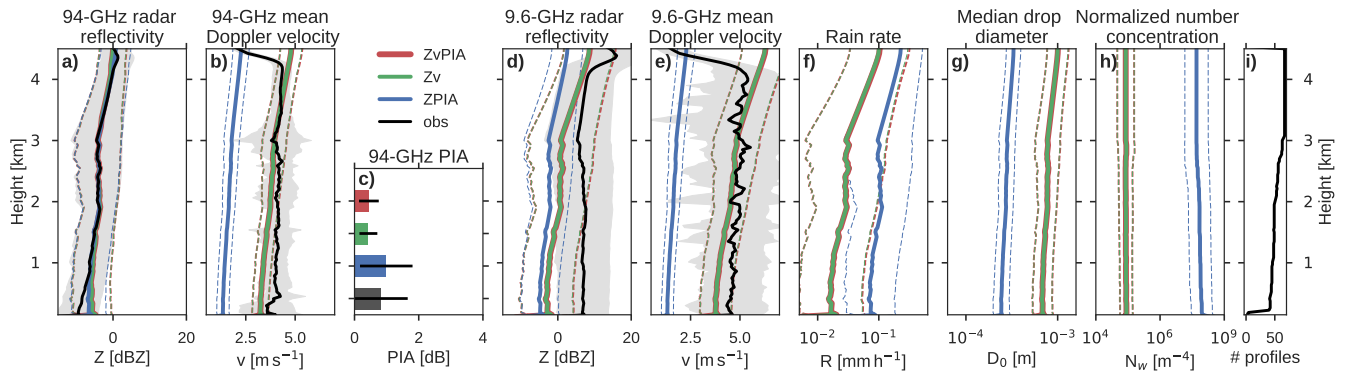


**Figure 9.** Averaged profiles of evaporating light rain between 13:12 and 13:17 on 22 July 2007. Forward-modelled 94 GHz radar reflectivity (a), mean Doppler velocity (b) and PIA (c); forward-modelled 10 GHz radar reflectivity (d) and mean Doppler velocity (e); and retrieved rain rate (f), median drop size (g), number concentration parameter (h) for ZPIA,  $Z_v$  and  $Z_v$ PIA retrievals. The number of profiles included at each height is indicated in (i). Shading and dashed lines indicate the  $1-\sigma$  standard deviation of the retrieved and derived variables.

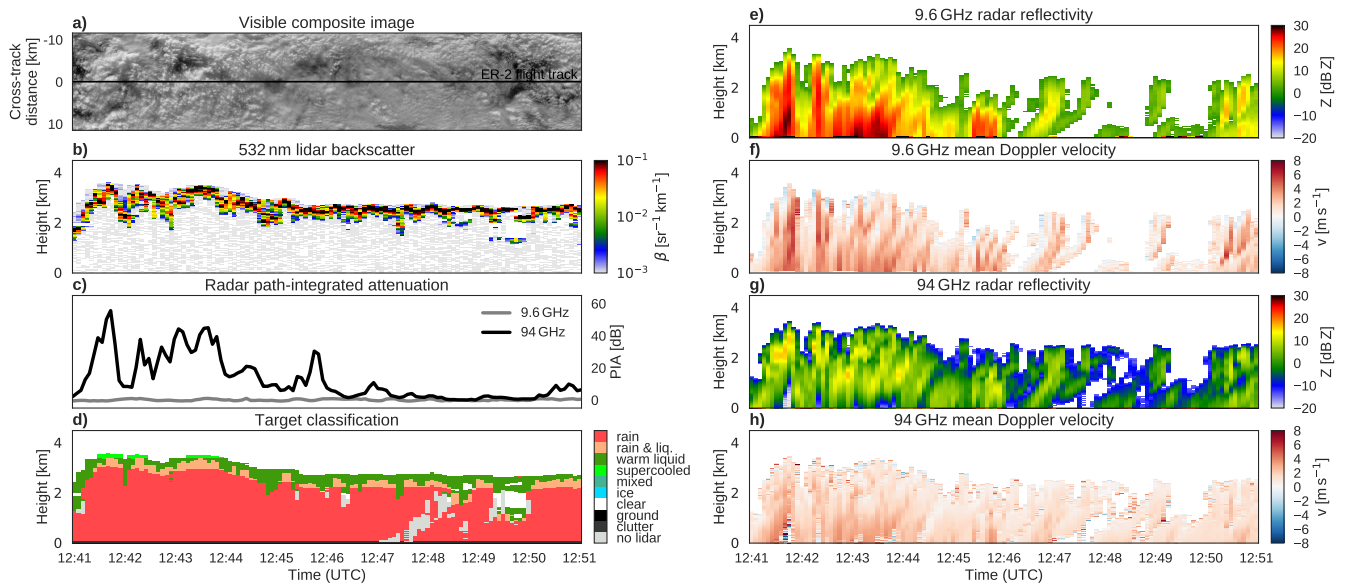


**Figure 10.** Selected measurements made by ER-2 instruments for Case 3 between 12:41 and 12:51 UTC on 29 July 2007 as part of TC4. Composite cloud scene (a) from MAS/MASTER visible channels, with the ER-2 flight track marked; 532 nm lidar backscatter (b); 9.6 and 94 GHz radar PIA (c); target classification from radar–lidar synergy (d); 9.6 GHz radar reflectivity (e) and mean Doppler velocity (f); and 94 GHz radar reflectivity (g) and mean Doppler velocity (h).

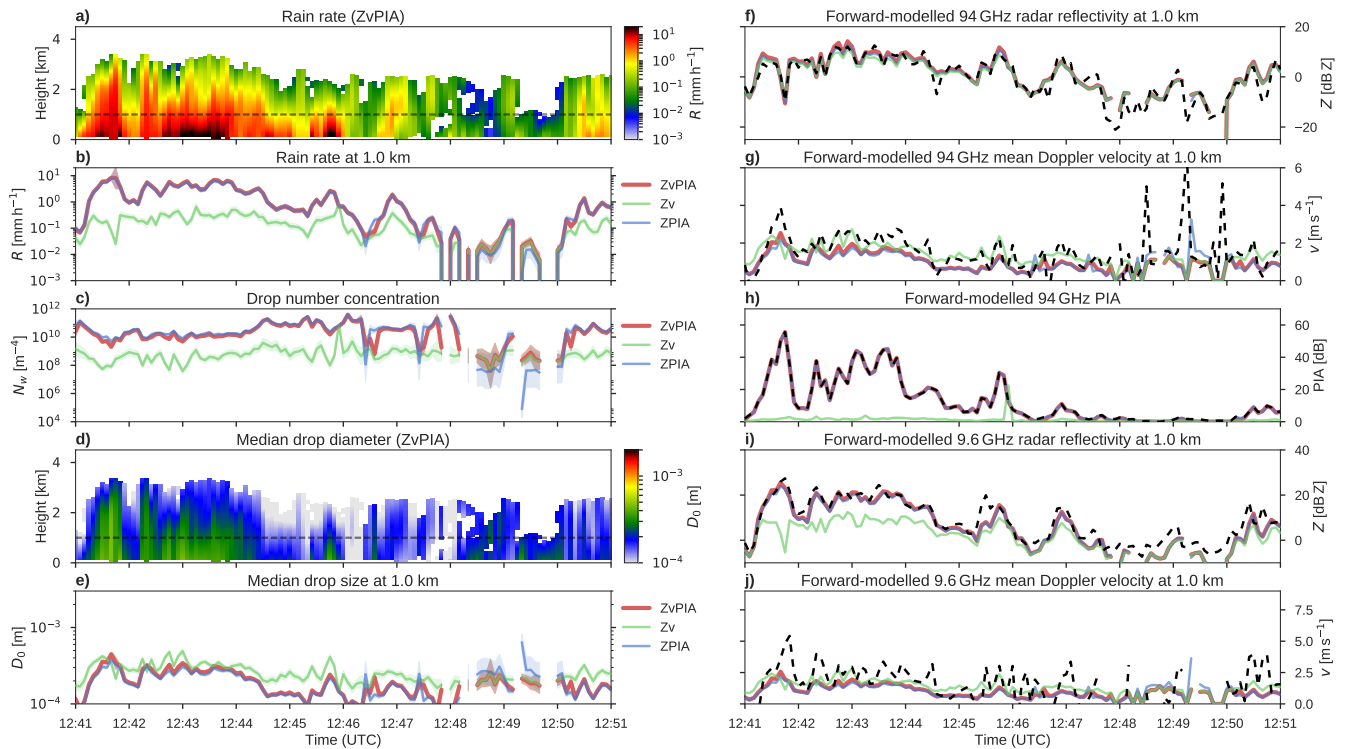


**Figure 11.** Time series of ZPIA, Zv and ZvPIA 94GHz retrievals for Case 3 on 29 July 2007. Retrieved state and derived variables (left), and forward-modelled radar measurements (right) for the three retrievals are shown at a height of 1 km above sea level (indicated with a light dashed line in the left-hand scenes), while full scenes of  $R$  (a) and  $D_0$  (d) are shown for the ZvPIA retrieval. Shading indicates the  $1-\sigma$  uncertainty in the retrieved and derived variables. Dark dashed lines (right) indicate the observed radar measurements.

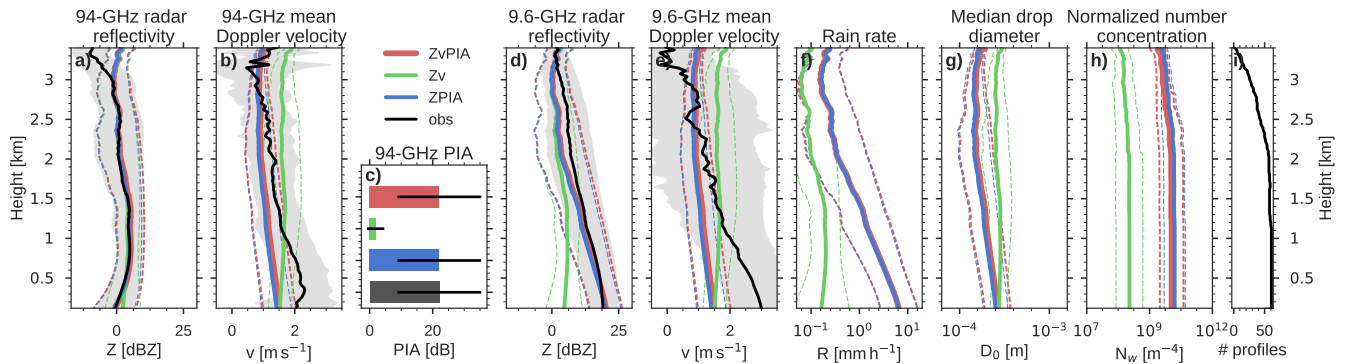


**Figure 12.** Averaged profiles of moderate rain between 12:41 and 12:46 UTC on 29 July 2007. Forward-modelled 94 GHz radar reflectivity (a), mean Doppler velocity (b) and PIA (c); forward-modelled 10 GHz radar reflectivity (d) and mean Doppler velocity (e); and retrieved rain rate (f), median drop size (g), number concentration parameter (h) for ZPIA, Zv and ZvPIA retrievals. The number of profiles included at each height is indicated in (i). Shading and dashed lines indicates the  $1-\sigma$  standard deviation of the retrieved and derived variables.

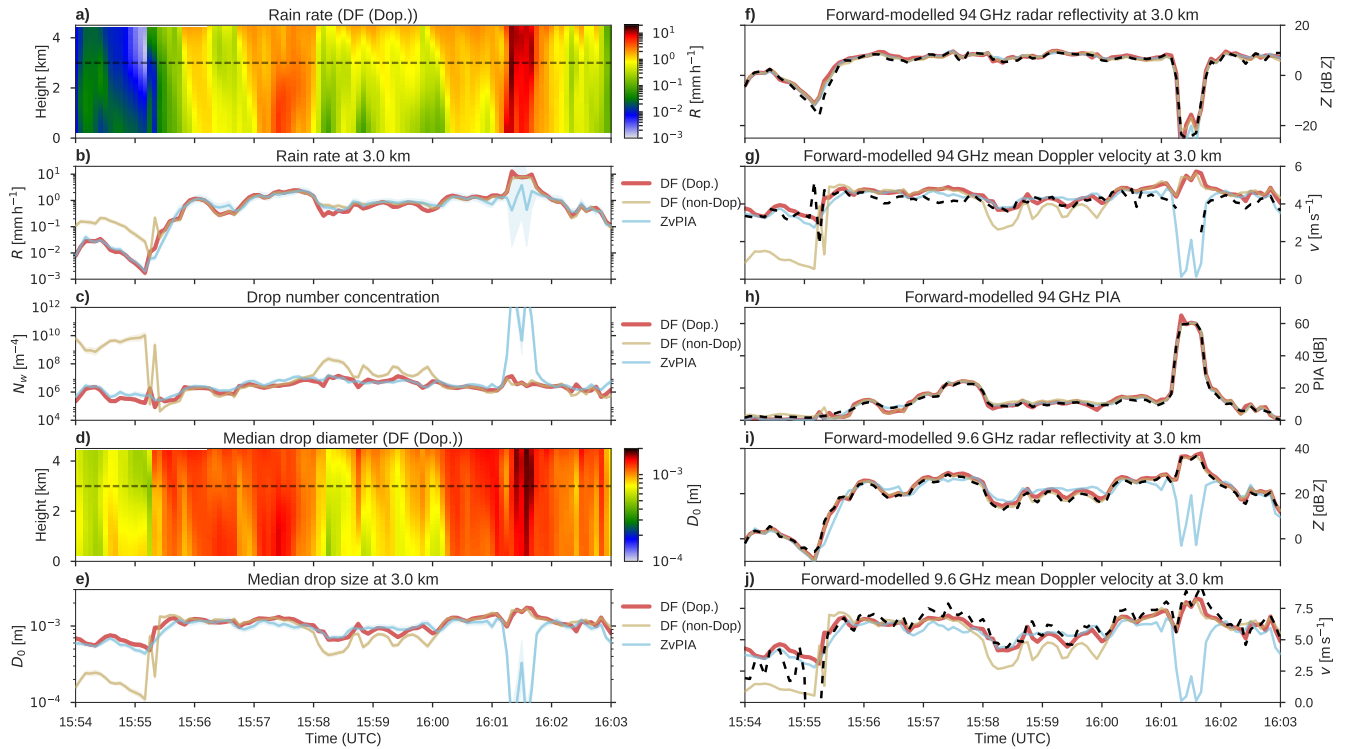


**Figure 13.** Time series of dual-frequency (DF) retrievals with and without Doppler, compared against the 94 GHz ZvPIA retrieval for Case 1 on 22 July 2007. Retrieved state and derived variables (left), and forward-modelled radar measurements (right) for the three retrievals are shown at a height of 3.0 km above sea level (indicated with a light dashed line in the left-hand scenes); while the full scenes of  $R$  (a) and  $D_0$  (d) are shown for the dual-frequency Doppler retrieval. Shading indicates the  $1\text{-}\sigma$  uncertainty in the retrieved and derived variables. Dark dashed lines (right) indicate the observed radar measurements.

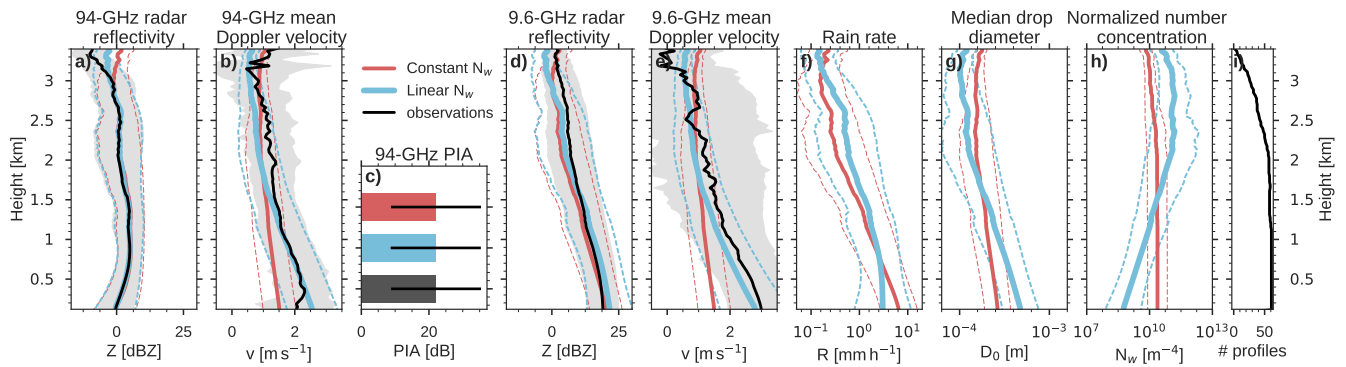


**Figure 14.** Averaged profiles of moderate rain between 12:41 and 12:46 UTC on 29 July 2007. Forward-modelled 94 GHz radar reflectivity (a), mean Doppler velocity (b) and PIA (c); forward-modelled 10 GHz radar reflectivity (d) and mean Doppler velocity (e); and retrieved rain rate (f), median drop size (g), drop number concentration parameter (h) for  $Zv$ PIA retrievals in which  $N_w$  is represented as a constant with height, and as a linear gradient. The number of profiles included at each height is indicated in (i). Shading and dashed lines indicate the  $1-\sigma$  standard deviation of the retrieved and derived variables.